Review in Advance first posted online on June 8, 2016. (Changes may still occur before final publication online and in print.)

Chemical Principles in Tissue Clearing and Staining Protocols for Whole-Body Cell Profiling

Kazuki Tainaka,[1] Akihiro Kuno,[2,3] Shimpei I. Kubota,[1] Tatzya Murakami,[1] and Hiroki R. Ueda[1,4]

[1]Department of Systems Pharmacology, The University of Tokyo, Tokyo 113-0033, Japan

[2]Department of Anatomy and Embryology, Faculty of Medicine, University of Tsukuba, Ibaraki 305-8575, Japan

[3]PhD Program in Human Biology, School of Integrative and Global Majors, University of Tsukuba, Ibaraki 305-8575, Japan

[4]Laboratory for Synthetic Biology, RIKEN Quantitative Biology Center, Suita, Osaka 565-0871, Japan; email: uedah-tky@umin.ac.jp

Annu. Rev. Cell Dev. Biol. 2016. 32:9.1–9.29

The *Annual Review of Cell and Developmental Biology* is online at cellbio.annualreviews.org

This article's doi:
10.1146/annurev-cellbio-111315-125001

Keywords

tissue clearing, fixation, permeabilization, decolorizing, RI matching, chemical staining

Abstract

Mammalian bodies have more than a billion of cells per cubic centimeter, which makes whole-body cell (WBC) profiling of an organism one of the ultimate challenges in biology and medicine. Recent advances in tissue-clearing technology have enabled rapid and comprehensive cellular analyses in whole organs and in the whole body by a combination of state-of-the-art technologies of optical imaging and image informatics. In this review, we focus mainly on the chemical principles in currently available techniques for tissue clearing and staining to facilitate our understanding of their underlying mechanisms. Tissue clearing is usually conducted by the following steps: (*a*) fixation, (*b*) permeabilization, (*c*) decolorizing, and (*d*) refractive index (RI) matching. To phenotype individual cells after tissue clearing, it is important to visualize genetically encoded fluorescent reporters and/or to stain tissues with fluorescent dyes, fluorescent labeled antibodies, or nucleic acid probes. Although some technical challenges remain, the chemical principles in tissue clearing and staining for WBC profiling will enable various applications, such as identifying cellular circuits across multiple organs and measuring their dynamics in stochastic and proliferative cellular processes, for example, autoimmune and malignant neoplastic diseases.

Contents

INTRODUCTION 9.2
STRATEGY FOR TISSUE CLEARING 9.7
FIXATION 9.9
Paraformaldehyde 9.10
Hydrogel Embedding 9.10
SWITCH-Based Glutaraldehyde 9.11
PERMEABILIZATION 9.11
Water-Miscible Polar Solvents 9.12
Hyperhydration Reagents without Delipidation 9.13
Delipidation Reagents 9.14
DECOLORIZING 9.16
REFRACTIVE INDEX MATCHING 9.17
PRESERVATION OF FLUORESCENT SIGNALS FROM REPORTER PROTEINS 9.18
STAINING OF ENDOGENOUS COMPONENTS 9.19
iDISCO 9.21
CUBIC 9.22
Sca*l*eS 9.22
CLARITY-Related Protocols 9.23
SWITCH 9.23
OUTLOOK 9.24

INTRODUCTION

An animal's body has an enormous number of cells that compose various functional and structural units. Different cell types play crucial roles in diverse physiological systems, including the respiratory and circulatory systems, nervous and skeletal/muscular systems, endocrine system, digestive system, and immune system. Comprehensive analysis of each system or organ at single-cell resolution in the body has been one of the most fundamental challenges in biology and medicine. Remarkable progress in imaging technology such as computed tomography (CT) (Bouxsein et al. 2010), magnetic resonance imaging (MRI) (Ogawa et al. 1990), positron emission tomography (PET) (Shokeen & Anderson 2009), and near infrared imaging (Leblond et al. 2010) has revealed detailed anatomical structures of living animals. However, it is still difficult to use these methods to extract various properties of individual cells due to the lack of high-contrast cell-labeling tools. Although conventional histology techniques are principally capable of global phenotyping of cells in fixed tissues (Isosaka et al. 2015, Oh et al. 2014, Ragan et al. 2012), these techniques are laborious and require tissue sectioning, which are challenging barriers to rapid three-dimensional (3D) visualization of organ structures. By contrast, optical projection tomography (Ntziachristos 2010, Sharpe 2004) and optical sectioning with light-sheet microscopy (Dodt et al. 2007, Keller et al. 2015) in combination with recent advances in tissue-clearing techniques (Susaki & Ueda 2016) are promising strategies toward visualizing single cells within a fixed whole-organ or whole-body context. Continuously updated informatics tools enable huge amounts of imaging data to be processed (Amat et al. 2015) and facilitate automated comparative analysis (Susaki et al. 2014, 2015), imaging processing (Chhetri et al. 2015), and information

extraction (Amat et al. 2014). Maturation of tissue clearing, rapid 3D imaging microscopy, and image informatics could provide novel biological and medical platforms for whole-body cell (WBC) profiling, allowing us to see both the forest and the trees (Economo et al. 2016, Keller & Ahrens 2015, Ode & Ueda 2015, Oh et al. 2014, Ragan et al. 2012).

Tissue clearing is the first critical step toward WBC profiling. A number of tissue-clearing reagents and protocols have been developed, as shown in **Table 1** and **Figure 1**. The pioneering work by Werner Spalteholz first introduced the principle of transparent 3D specimens a century ago (Spalteholz 1914). Dodt and colleagues built upon Spalteholz's achievements by applying a benzyl alcohol/benzyl benzoate (BABB)-based clearing protocol to their original ultramicroscopy, which enabled rapid 3D imaging of whole organs based on light-sheet fluorescence microscopy (LSFM) (Dodt et al. 2007). Subsequently, Dodt and colleagues explored GFP-friendly organic solvents from a large library of more than 10,000 chemicals and discovered highly effective ones in tetrahydrofuran (THF) and dibenzylether (DBE) (Becker et al. 2012). These protocols are summarized as 3DISCO (Ertürk et al. 2012). The Tessier-Lavigne group has established a rapid whole-mount staining protocol termed iDISCO, which is based on 3DISCO (Renier et al. 2014). In addition to conventional hydrophobic organic chemical cocktails, hydrophilic reagents—including sugars (e.g., glucose), alcohols (e.g., glycerol, polyethylene glycol, butanediol, trimethylolpropane, sorbitol, xylitol), dimethyl sulfoxide (DMSO), and oreic acid—have been used (Susaki & Ueda 2016, Tuchin 2015). Recently, the Imai group developed a clearing method termed SeeDB, which is based on fructose (Ke et al. 2013). The Miyawaki group used hyperhydration urea (Hama et al. 2011), which led to other urea-based clearing protocols, including CUBIC (Susaki et al. 2014), FRUIT (Hou et al. 2015), ClearSee (Kurihara et al. 2015), and Sca*l*eS (Hama et al. 2015). Sca*l*eS, which uses both urea and sorbitol, has improved clearing performance without disturbance of intact cell structures. In contrast to Sca*l*eS, CUBIC sought to promote more effective delipidation to ensure sufficient clearance of specimens so that whole-organ images at single-cell resolution could be acquired by LSFM. Aminoalcohols in the CUBIC cocktail had an unexpected decolorizing ability, resulting in clearance of blood-infused tissue in addition to efficient lipid solubility (Tainaka et al. 2014) and thus enabling 3D anatomy and pathology of various organs at single-cell resolution by rapid whole-body and whole-organ imaging. The Deisseroth group developed CLARITY, which is a combination of hydrogel-embedding fixation and electrophoretic delipidation (Chung & Deisseroth 2013, Chung et al. 2013). Endogenous proteins were well preserved by covalent cross-linking in an acrylamide gel. Delipidation by the ionic detergent was dramatically accelerated by the electric field potential. More recently, CLARITY was improved by various related techniques, including PACT-PARS (Yang et al. 2014), stochastic electrotransport–based clearing (Kim et al. 2015), CLARITY-TDE (Costantini et al. 2015), and ACT-PRESTO (Lee et al. 2016). The Gradinaru group has also greatly advanced these detergent-based clearing protocols and has provided many fruitful applications, including optimization of hydrogel-based fixation, passive delipidation (PACT), perfusion-based delipidation (PARS), highly effective RI adjustment (RIMS), decalcification (PACT-deCAL), and tissue clearing through expansion (ePACT) (Treweek et al. 2015, Yang et al. 2014). The Chung group has strongly contributed to versatile staining principles based on stochastic electrotransport and binding-controlled passive diffusion in a development termed SWITCH, which is backed by well-founded theory (Kim et al. 2015, Murray et al. 2015).

All current techniques result in tissue clearing by similar physical principles, despite different chemical approaches. However, as far as we know, the underlying chemical principles have not been highlighted. In this review, we mainly discuss the chemical principles for major clearing protocols and introduce emerging chemical staining methods.

Table 1 Tissue-clearing protocols for mammalian samples

Reference	Protocol	Fixation	Permeabilization	Decolorizing	RI match	RI	Clearing performance
Dodt et al. 2007, Schwarz et al. 2015	BABB	PFA	EtOH, 1-PrOH, or *t*-BuOH: dehydration; CH_2Cl_2: delipidation	None	BABB	1.56	High (3–4)
Becker et al. 2012, Ertürk et al. 2012, Renier et al. 2014	3DISCO, iDISCO	PFA	THF: dehydration and delipidation; CH_2Cl_2: delipidation	H_2O_2: heme and other chromophores	DBE	1.56	Highest (5)
Aoyagi et al. 2015, Costantini et al. 2015	TDE	PFA	TDE: dehydration	None	TDE	1.48–1.52	Moderate (1)
Kuwajima et al. 2013	*Clear*^{T}, *Clear*^{T2}	PFA	Formamide: dehydration or formamide-induced molecular influx	None	Formamide/ polyethylene glycol	1.45	Moderate (1)
Hama et al. 2011	Sca*l*e	PFA	Sca*l*eA2 (urea/glycerol/Triton X-100) ■ Urea: hydration and molecular influx	None	Sca*l*eA2	1.38	Moderate (1)
Hou et al. 2015	FRUIT	PFA	FRUIT (urea/fructose) ■ Urea: hydration and molecular influx ■ Fructose: osmotically balanced molecular flux	Thioglycerol: Maillard reaction	FRUIT	1.46–1.50	Moderate (1–2)
Hama et al. 2015	Sca*l*eS	PFA	Sca*l*eS (urea/sorbitol/DMSO): ■ Urea: hydration and molecular influx ■ Sorbitol: osmotically balanced molecular flux	None	Sca*l*eS4 (urea/ sorbitol/ DMSO)	1.44	High (2–3)
Ke et al. 2013	SeeDB	PFA	Fructose: osmotically balanced molecular flux	Thioglycerol: Maillard reaction	Fructose	1.49	Moderate (1)
Ke et al. 2016	SeeDB2	PFA	Saponin: delipidation	None	Histodenz^{TM}	1.52	High (2–3)
Susaki et al. 2014, 2015; Tainaka et al. 2014	CUBIC	PFA	Sca*l*eCUBIC-1 (urea/aminoalcohol/Triton X-100): ■ Urea: hydration and molecular influx ■ Aminoalcohol/Triton X-100: delipidation	Aminoalcohol: heme	Sca*l*eCUBIC-2 (urea/ aminoalcohol/ sucrose)	1.49	High (3–4)

Susaki & Ueda 2016; **http://cubic.riken.jp**	CUBIC	PFA	Sca/eCUBIC-1A (urea/aminoalcohol/Triton X-100/NaCl): ■ Urea/NaCl: osmotically balanced molecular flux ■ Aminoalcohol/Triton X-100: delipidation	Aminoalcohol: heme	Sca/eCUBIC-2 (urea/aminoalcohol/sucrose)	1.49	High (3-4)
Economo et al. 2016		PFA	Sca/eCUBIC-1 (urea/aminoalcohol/Triton X-100): ■ Urea: hydration and molecular influx ■ Aminoalcohol/Triton X-100: delipidation	Aminoalcohol: heme	DMSO/sorbitol	1.47	High (3–4)
Chung et al. 2013, Tomer et al. 2014	CLARITY	PFA/acrylamide/bis-acrylamide	Passive clearing or ETC-based clearing SDS: delipidation	SDS: heme	FocusClear™; glycerol; RI 1.454 category 1806Y (Cargille Labs)	1.45	Passive clearing: high (3–4); ETC: highest (4–5)
Treweek et al. 2015, Yang et al. 2014	PACT-PARS	PFA, acrylamide	Passive clearing (PACT) or perfusion-based clearing (PARS) SDS: delipidation	SDS: heme; Sudan Black B: lipofuscin autofluorescence	RIMS: Histodenz™; sRIMS: sorbitol	RIMS: 1.46–1.49; sRIMS: 1.44	PACT: high (3); PARS: highest (3–5)
	ePACT	(*1*) PFA, (*2*) acrylamide/bis-acrylamide/sodium acrylate	SDS: delipidation Collagenase: fiber digestion	None	Deionized water	1.33	
Costantini et al. 2015	CLARITY-TDE	PFA/acrylamide/bis-acrylamide	ETC-based clearing SDS: delipidation	SDS: heme	TDE	1.45	Highest (4–5)
Kim et al. 2015	Stochastic electrotransport	PFA/acrylamide/bis-acrylamide	ETC-based clearing SDS: delipidation	SDS: heme	Diatrizoic acid/*N*-methylglucamine/sorbitol	1.46	Highest (5)
Chen et al. 2015	Expansion microscopy	(*1*) PFA, (*2*) acrylamide/bis-acrylamide/sodium acrylate	Protease: fiber digestion	None	Deionized water	1.33	
Murray et al. 2015	SWITCH	Glutaraldehyde	Thermal clearing SDS: delipidation	Thioglycerol or sodium sulfite: Maillard reaction	Diatrizoic acid/*N*-methylglucamine/iodixanol	1.47	Highest (5)

Abbreviations: BABB, benzyl alcohol/benzyl benzoate; DBE, dibenzylether; DMSO, dimethyl sulfoxide; ETC, electrophoretic tissue clearing; PFA, paraformaldehyde; RI, refractive index; SDS, sodium dodecyl sulfate; TDE, 2,2′-thiodiethanol; THF, tetrahydrofuran.

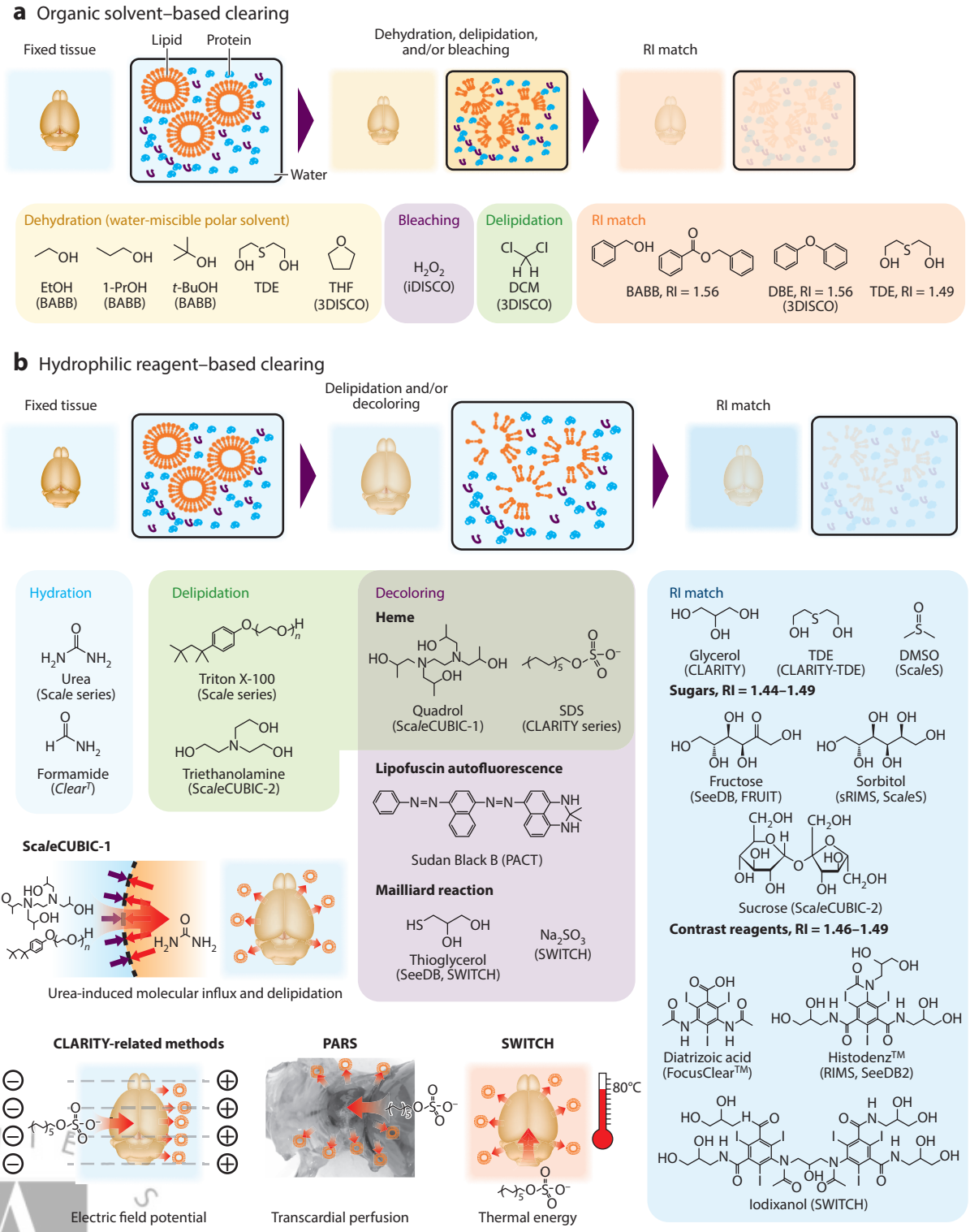

STRATEGY FOR TISSUE CLEARING

The opacity of biological tissues is derived from heterogeneous components with different optical properties such as refractive index (RI) and light absorption (Tuchin 2015, Tuchin et al. 1997). Most biological tissues are composed of 70–80% water with low RI ($n = 1.33$), ~10% proteins with high RI ($n > 1.44$), and ~10% lipids with high RI ($n > 1.45$) (Johnsen & Widder 1999, Tuchin 2015). Incoming light is scattered by the heterogeneity in the RIs of these components. In addition, light transmission decays by light absorption from endogenous pigments such as heme, riboflavin, melanin, and lipofuscin (Horecker 1943, Tuchin 2015, Weissleder 2001). In this review, we focus on the chemical principles of tissue clearing: how various chemicals can reduce both light scattering and light absorption. For more detailed discussion of the underlying physics of tissue clearing, the reader is referred to reviews by Johnsen & Widder (1999) and Tuchin (2015). Tissue-clearing protocols should achieve homogenization of RI inside tissues and removal of endogenous absorbents without loss or disruption of molecules of interest. Tissue clearing is usually conducted by the following steps: (*a*) tissue fixation, (*b*) permeabilization, (*c*) decolorizing, and (*d*) RI matching by high-RI medium (**Figure 1**). Most currently available clearing protocols have been developed to visualize specific proteins inside tissues via encoding of fluorescent reporter proteins or postlabeling by fluorescently tagged antibodies.

In the first step, researchers should consider tissue fixation methods suitable for protein retention through the tissue-clearing protocol (**Figure 2**). If more efficient tissue fixation conditions are chosen to retain proteins more rigidly, tissue-clearing conditions must become harsher. Because water molecules occupy 70–80% of the volume of tissues and exhibit much lower RI than do proteins, water inside tissues has to be substituted with a high-RI medium in the homogenization process of RI (Liu et al. 1996, Tuchin 2015, Tuchin et al. 1997). Lipids also cause light scattering inside tissue due to high RI. In addition, lipids, which are the major component of the plasma membrane, obstruct external medium from cells. Therefore, delipidation is also an important process to permeabilize cell membranes and therefore render full clearing of tissues so that whole-organ samples can be visualized by LSFM with single-cell resolution. Small pigments such as heme can be eliminated from tissues by several clearing conditions (Lee et al. 2014, Tainaka et al. 2014, Yang et al. 2014). Although it is still hard to remove large pigments such as melanin and lipofuscin, some chemical treatments may suppress autofluorescence from lipofuscin in elderly mammalian brain samples (Treweek et al. 2015). Additionally, several chemical treatments, such as those by the Maillard reaction, result in undesirable coloring. Reductive chemical treatment partially solves these problems (Ke et al. 2013, Murray et al. 2015).

Chemically speaking, current tissue-clearing protocols are divided into two groups: organic solvent–based clearing methods and hydrophilic reagent–based clearing methods (**Figure 1**). In the former, dehydration and permeabilization occur through alcohol or ether treatment (Dodt

Figure 1

Overview of tissue-clearing methods. (*a*) Organic solvent–based clearing methods include dehydration, delipidation, bleaching, and refractive index (RI) matching. Water-miscible polar solvents dehydrate tissue samples. Delipidation by THF or DCM contributes to clearing efficiency after RI matching. Although the water-free clearing method results in some tissue shrinkage and quenching of fluorescent proteins, these protocols are simple and fast and have high clearing performance. (*b*) Hydrophilic reagent–based clearing methods include delipidation, decolorizing, and RI matching. Detergents and aminoalcohols remove lipids from tissue samples. Delipidation is facilitated by chemically or physically induced molecular flux. Urea promotes the influx of aminoalcohol and detergent in the CUBIC protocol. Permeation of the ionic detergent SDS is driven by electric field potential (CLARITY), transcardial perfusion (PARS), or thermal energy (SWITCH). Highly water-soluble molecules such as sugars and contrast reagents are used as RI matching medium.

et al. 2007, Ertürk et al. 2012). Those solvents are miscible in organic solvent, and thus high-RI aromatic solvents ($n \sim 1.56$) homogeneously fill the tissue. This approach has an advantage in clearing kinetics probably due to the effective diffusion coefficient of small molecules. In contrast, organic solvents are often harmful and attenuate fluorescent reporters. Although pretreatment of basic solution alleviates some quenching of fluorescent proteins (Schwarz et al. 2015), harmful

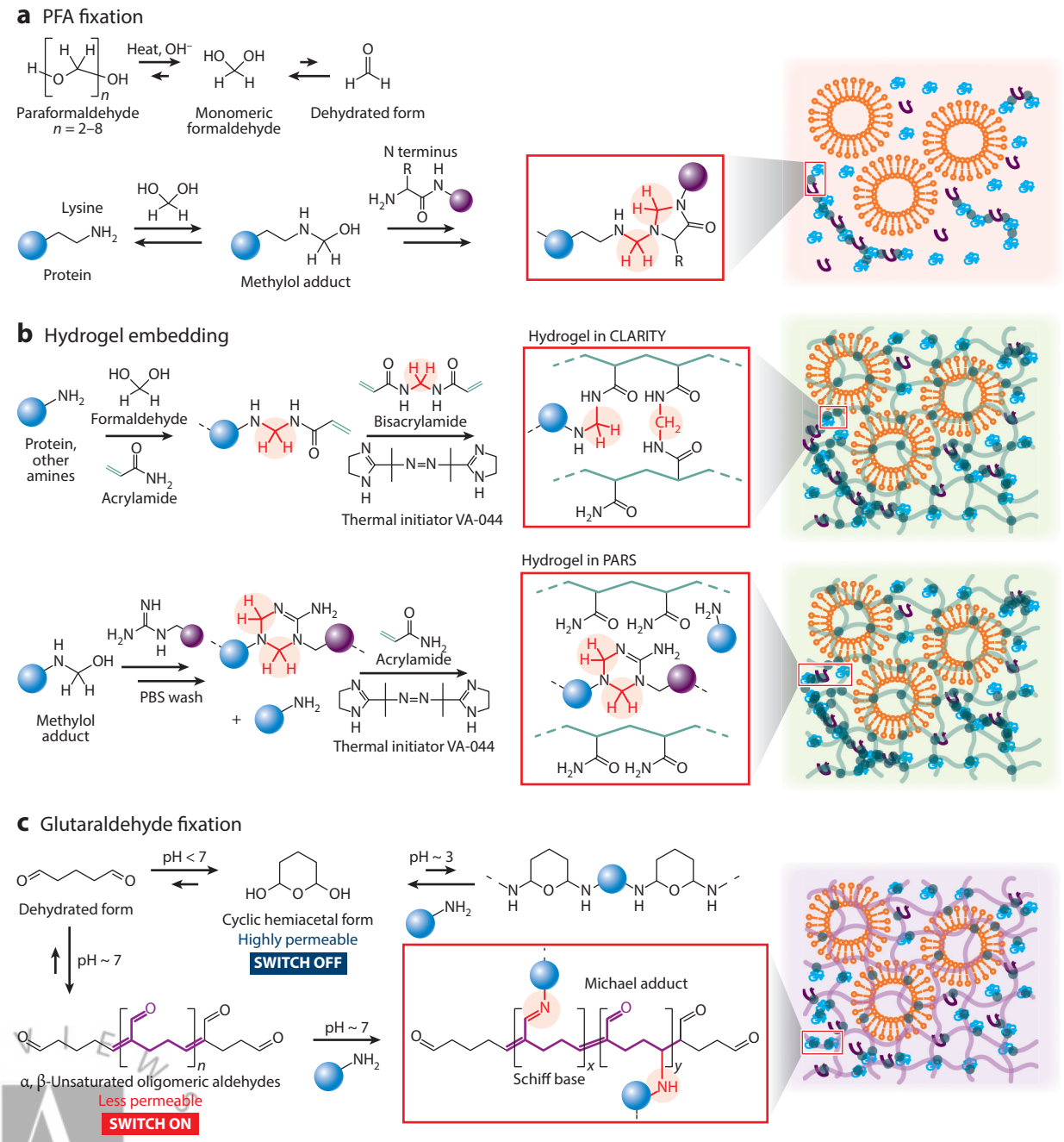

waste, especially explosive THF and DBE, remain a problem. In the latter hydrophilic method, fully cleared tissue samples are prepared by detergent-based delipidation and by RI matching with a concentrated sugar- or contrast agent–based aqueous medium with high RI ($n \sim 1.44$–1.49). This approach is appropriate for visualization of endogenous fluorescent proteins and is relatively harmless in spite of redundant and laborious protocols. All current clearing protocols have both advantages and disadvantages, so users should determine the protocol best suited for their purpose.

FIXATION

Tissue fixation is a fundamental step to preserve molecules of interest during the tissue-clearing process. Most clearing protocols aim for visualization of intracellular proteins, and therefore conventional fixation protocols were based on protein-specific chemical reactions, except for several coagulant fixations such as trichloroacetic acid (Hirashima & Adachi 2015). Recently, hydrogel-based and glutaraldehyde-based fixation methods have succeeded in the preservation of lipids and even small molecules such as GABA and dopamine (Chung et al. 2013, Murray et al. 2015). The Deisseroth group has revealed that postfixation of hydrogel-emmbedded tissues by 1-ethyl-3-(3-dimethylaminopropyl)carbodiimide (EDC) significantly enhanced preservation of transcriptional products by cross-linking of the 5′-phosphate group of RNA molecules (Sylwestrak et al. 2016). The Briggman group has demonstrated that an osmolarity-balanced fixative buffer contributes to preservation of extracellular space (Pallotto et al. 2015). Before describing representative fixation chemistry, we summarize key considerations for the relationship between fixation and clearing as follows.

1. Basic amino groups such as lysine are largely consumed (depending on the degree of fixation) by the cross-link reaction during all chemical fixation processes. Thus, isoelectric points of biomolecules inside fixed tissues are shifted in the acidic direction. Because biomolecules such as proteins, lipids, and nucleic acids tend to be insoluble in acidic conditions, chemical clearing is more favorable in neutral to basic conditions.
2. More highly fixed tissues require harsher clearing conditions to be fully transparentized. Thus, researchers should choose a chemical fixation depending on the research purpose and the available equipment. For example, to visualize signals from relatively abundant fluorescent proteins in mice organs without specific devices such as an electrophoretic tissue-clearing chamber, paraformaldehyde (PFA) or PACT fixation is more feasible because this protocol clears tissue by simple immersion. In contrast, SWITCH-based glutaraldehyde fixation is more desirable for minimizing protein loss to detect tiny amounts of proteins in human organs by immunohistochemistry.
3. Generally, chemical fixation induces artificial and multiple chemical reactions in biological systems. Architectures in the living organism are altered not only by the clearing process but also by the initial fixation process.

Figure 2

Fixation chemistry of paraformaldehyde (PFA), hydrogel embedding, and SWITCH-based glutaraldehyde. Illustrated are plausible mechanisms in covalent cross-link reaction. (*a*) In PFA fixation, monomeric formaldehyde prepared from polymerized PFA can activate basic amino acids of proteins to yield methylol adducts, which then condense with other functional groups such as N-terminal amino groups. (*b*) CLARITY hydrogels can form covalent cross-links between polymerized protein networks and acrylamide gel matrices, whereas these are independent in PARS hydrogels. (*c*) In glutaraldehyde chemistry, highly permeable cyclic hemiacetal is predominant at approximately pH 3 and is inert to acidic polymerization (SWITCH OFF). At approximately pH 7, glutaraldehyde is polymerized to form less permeable α,β-unsaturated oligomeric aldehydes (SWITCH ON). Oligomeric aldehydes react with proteins via Schiff base and Michael-type reactions.

Paraformaldehyde

PFA is one of the most widely used fixative reagents. Because monomeric PFA is a tiny molecule, PFA is highly permeable in tissues. In the initial step, aldehyde rapidly reacts with basic amino groups such as lysine and N-terminal amino groups of endogenous proteins to form methylol adducts (Metz et al. 2004, 2006) (**Figure 2**). This step is reversible and considered to be completely finished within 24 h at 4°C (Helander 1994). Thus, methylol adducts can be restored to the original amino groups and free aldehyde by washing with phosphate-buffered saline (PBS). In the second step, the methylol adducts are irreversibly conjugated with adjacent arginine, histidine, tyrosine, tryptophan, asparagine, glutamine, and N-terminal amino groups of proteins. Cross-linking between arginine and tyrosine, in the Mannich reaction, can be recovered by several antigen retrieval conditions (Sompuram et al. 2004). This latter cross-link reaction is relatively slow and may not be completely finished in the short postfixation period in current clearing protocols. Because PFA fixation is insensitive to lipids, lipids are efficiently washed out by detergent-based delipidation. In addition, PFA forms only physically contiguous protein networks and fails to covalently fix spatially isolated proteins. To observe tiny amounts of proteins, researchers should use other fixative methods that more effectively preserve protein. However, PFA fixation accelerates tissue clearing under relatively mild conditions and is therefore suitable for preparing fully cleared specimens that retain signal from fluorescent proteins.

Hydrogel Embedding

The Deisseroth group developed a novel fixation method by hydrogel embedding, which improved the preservation efficiency of proteins by covalent conjugation with an acrylamide gel matrix (Chung et al. 2013). Initially, anesthetized mice or other mammalian organisms are perfused with a chemical cocktail of PFA, an acrylamide monomer (a mixture of acrylamide and *N*,*N*′-methylene bisacrylamide), and a thermal polymerization initiator. Methylol adducts between amino groups of proteins and aldehyde form after 1 day after fixation at 4°C (**Figure 2**). During the initiation of polymerization at 37°C, the embedded acrylamide polymerizes in a gel matrix, and methylol adducts are covalently attached to the amide group of acrylamide. Unlike PFA fixation, the hydrogel embedding fixation preserves spatially isolated proteins in the gel matrix and enhances the physical and chemical strength of the specimens. However, because this fixation also noncovalently retains lipids in the gel matrix, it is necessary to apply an electric field potential in the presence of the strong detergent SDS to remove lipids. The Gradinaru group investigated milder clearing conditions to clear the whole mouse body, including fragile tissues, and found the minimal fixation suitable for SDS-based passive clearing (Treweek et al. 2015, Yang et al. 2014). As a result, this group demonstrated that SDS-based passive clearing is compatible with effective protein preservation by only a 4% acrylamide-based fixative without bisacrylamide as a cross-linker. We noted that SEM images showed that pore sizes of 4% acrylamide matrices were larger than those of 4% PFA-acrylamide matrices (Yang et al. 2014). Therefore, antibodies more deeply penetrated into 4% acrylamide matrices than into 4% PFA-acrylamide matrices. In this fixation, the weight and volume of tissue-hydrogel matrices after SDS-based delipidation swelled approximately twofold. But those specimens shrank to their original sizes without significant anatomical distortion after RIMS treatment as an RI-matching step.

The Boyden group devised an alternative hydrogel-embedding method for linear tissue expansion that led to an increase in optical resolution: expansion microscopy (EM) (Chen et al. 2015). Thin brain slices were embedded into a hydrogel composed of sodium acrylate, which is well-known water absorptive polymer, and acrylamide. Those slices underwent a 4.5-fold linear

expansion without distortion after proteolytic treatment and deionization with distilled water. We noted that intensive tissue swelling by water is accompanied by the reduction of RI inside tissues (Chen et al. 2015). Thus, this approach is another strategy for tissue clearing without high-RI homogenization. EM requires complicated labeling methods to visualize target proteins due to the proteolysis treatment. To address this issue, the Gradinaru group treated acrylate/acrylamide-embedded rodent brain slices with collagenase in place of protease in addition to SDS-based delipidation; this protocol was termed ePACT (Treweek et al. 2015). This protocol succeeded in expanding slices up to fourfold to visualize Thy1-YFP signals. Despite several distorted cellular architectures, this protocol is a promising approach for scalable visualization ranging from a macroscopic view of tissue slices to a microscopic image with subcellular resolution.

SWITCH-Based Glutaraldehyde

Glutaraldehyde is also commonly used for intermolecular cross-linking of endogenous proteins (Hopwood 1972). The fixing effect of the bifunctional aldehyde is stronger than that of PFA. However, it is hard to homogeneously fix thick tissues by the fixative due to its low permeability (Hopwood 1967). The Chung group has discovered that glutaraldehyde can penetrate through large organs such as rat and marmoset brains under nonreactive acidic buffer (pH $\sim$ 3) and can rapidly initiate cross-link reactions inside deeper regions of tissues by replacement in reactive neutral buffer (pH $\sim$ 7), in a process termed SWITCH (Murray et al. 2015) (**Figure 2**). The SWITCH-based glutaraldehyde fixation is physically and chemically the most stable among all fixatives compatible with tissue clearing. Interestingly, this fixation also preserves some lipids and even small molecules such as dopamine after clearing. Glutaraldehyde-fixed tissues are delipidated by boiling at 80°C in aqueous clearing solution containing 200 mM SDS. Nevertheless, due to the rigid fixation, the intensive treatment does not result in significant loss of proteins or in antigenicity.

PERMEABILIZATION

Permeabilization is an essential step for promoting the substitution of water inside tissues with high-RI medium. In this step, cell-permeable molecules are substituted for water driven by osmotic pressure at high concentration (**Figure 3**). Alternatively, lipids—barriers to molecular flux—are removed to facilitate passive diffusion of external molecules into tissues (**Figure 1**). Swelling-shrinking behavior of tissues under each chemical treatment may be helpful for understanding the underlying molecular mechanisms of permeabilization. Most permeabilizing reagents in current protocols could be categorized into one of three groups: (*a*) water-miscible polar solvents, (*b*) hyperhydration reagents without delipidation, or (*c*) delipidation reagents. The delipidation part includes several strategies for active detergent influx into tissues; one example is electric field potential, which is utilized in CLARITY. According to previous clearing results, fixed tissues could be fully transparentized by thorough delipidation. Generally, permeabilization by polar solvents or delipidation reagents provides much clearer specimens than that by hyperhydration reagents without delipidation. Thus, the former reagents are appropriate for comprehensive macroscopic analysis such as whole-organ or whole-body imaging by LSFM. In contrast, the latter reagents without delipidation, such as urea and sugar, specialize in the preservation of precise cellular architecture and so are suitable for detailed microscopic observation with subcellular resolution by multiphoton fluorescent microscopy.

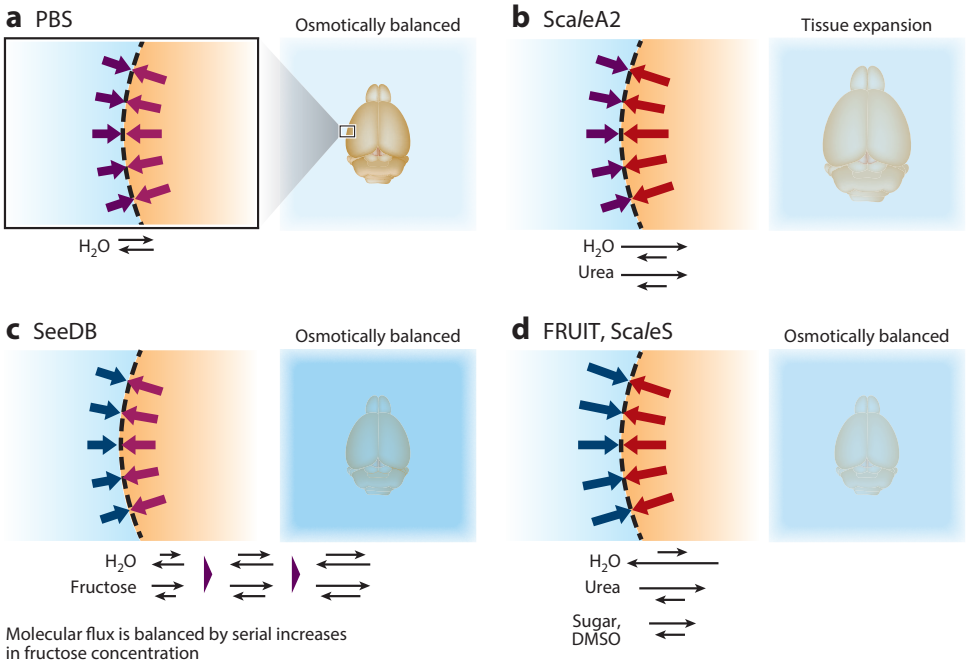

Figure 3

Plausible mechanisms in permeabilization without delipidation by hyperhydration reagents. (*a*) Brain tissues in PBS are osmotically balanced. (*b*) In the Sca*l*eA2 protocol, highly permeable urea may initiate the import of external water molecules by increasing internal osmotic pressure. (*c*) In the SeeDB protocol, osmotic dehydration can be adequately balanced with permeation of fructose by controlling gradual increases in fructose concentration. (*d*) FRUIT and Sca*l*eS achieve rapid clearing of brain tissues without significant deformation by means of the osmotically balanced potentiation of molecular flux across tissues.

Water-Miscible Polar Solvents

High-RI ($n > 1.5$) aromatic solvents are immiscible with water, whereas water-miscible polar solvents such as alcohols and THF are miscible with both aromatic solvents and water in any proportion (**Figure 1**). Therefore, solvents can play an essential role in mediating the substitution of water with high-RI aromatic solvents inside tissues. Classically, biological tissues were dehydrated by alcohols (Spalteholz 1914). In an early protocol from the Dodt group, tissues were dehydrated by serially increasing the EtOH concentration up to 100% and rinsing with 100% hexane (Dodt et al. 2007). EtOH is small enough to be rapidly replaced with water by passive diffusion. Water composes 70–80% of major tissues, forms 3D hydrogen-bonding networks with intracellular constituents, and creates space inside tissues (Pal et al. 2002, Zimmerman & Minton 1993). EtOH has much less hydrogen bonding ability than water. Thus, EtOH-solvated tissues are shrunk and hardened after dehydration. Recently, Ertürk et al. (2012) pointed out that the EtOH-BABB clearing protocol failed to clear myelinated tissues such as the adult mouse brain. So EtOH may be insufficient for tissue delipidation. The Dodt group screened more than 10,000 chemicals to find a highly effective and GFP-friendly dehydrating reagent, THF (Becker et al. 2012). This polar ether–based 3DISCO protocol has achieved extremely rapid dehydration due to its high permeable kinetics and has provided fully cleared organ samples after RI matching. Because THF has significant lipophilicity (Díaz et al. 1992), this protocol may accompany highly

effective delipidation. THF-solvated tissues are more slightly shrunk than EtOH-solvated ones, probably because THF lacks donating hydrogen. After mounting in DBE, tissues become rapidly cleared without further shrinkage. The Nemoto group and the Pavone group have investigated another water-miscible polar solvent, 2,2′-thiodiethanol (TDE) as a clearing medium (Aoyagi et al. 2015, Costantini et al. 2015). TDE has also been utilized as a water-miscible mounting medium because of its high RI ($n = 1.52$), which is equivalent to that of glass and typical immersion oils (Staudt et al. 2007). So TDE can be expected to combine the chemical properties of both dehydration and RI matching. However, adult mice brains were not fully transparentized and significantly shrunk after 60% or 97% TDE treatment (Aoyagi et al. 2015). This result may be attributed to the relatively slow kinetics of TDE influx. The clearing performance by TDE could be potentially improved by alterations in protocol such as serially increasing TDE concentration or combining hyperhydration reagents as described below. Overall, permeabilization by polar solvents is a feasible strategy for tissue clearing, but with the drawbacks of handling of harmful chemicals and quenching of fluorescent proteins.

Hyperhydration Reagents without Delipidation

Among hyperhydration reagents, the Miyawaki group discovered the clearing ability of an aqueous urea–based solution termed Sca*l*e (Hama et al. 2011). Although the cell membrane limits molecular flux, small, uncharged molecules can quickly pass through the lipid bilayer (Petty 1993). A small, uncharged urea molecule (with molecular weight = 60 and molecular radius = 0.22 nm) is one of the most permeable molecules and has strong hyperhydration abilities due to its bearing both hydrogen donor and acceptor groups. Also, urea is a relatively weak denaturant for proteins and nucleic acids because it disturbs their hydrogen-bonding networks (Hua et al. 2008, Priyakumar et al. 2009). Furthermore, urea increases membrane fluidity (Barton et al. 1999, Feng et al. 2002) to enhance molecular flux across membranes and retain chemicals in cells (Bentley et al. 1997). The optimized Sca*l*eA2 cocktail contains 4 M urea, 10% glycerol, and 0.1% nonionic detergent Triton X-100. Once biological tissues are immersed in Sca*l*eA2, tissues begin to swell and optically clear. One possible hypothesis for tissue expansion is that urea relaxes protein scaffolds involving solid tissue frameworks such as collagen fibers (Usha & Ramasami 2002), as shown in the dramatic expansion of collagenase-treated, hydrogel-embedded tissues in ePACT (Treweek et al. 2015). As a result, solvation of dense fiber proteins could lead to reduced light scattering inside tissues. In addition, the inside osmotic pressure would be increased, thereby inducing influx of outer molecules, including water and other ingredients (**Figure 3**). If so, the ionic gradient between internal and external tissue would also be important in the molecular flux and optical clearing by urea (Hou et al. 2015). Actually, ionic contamination significantly suppresses both tissue expansion and clearing by Sca*l*eA2. Furthermore, aqueous guanidine solution, which is similar to urea but is an ionic chaotrope (Greene & Pace 1974), displayed much less clearing in brain tissues and shrank tissues (T. Murakami & H.R. Ueda, unpublished results). This hypothesis of increased internal osmotic pressure may also be supported by the empirical observation that tissues swollen due to Sca*l*eA2 immediately shrank to nearly their original size after PBS washing. We also note that clearing by urea-based cocktails does not accompany lipid removal inside tissues unless delipidation chemicals like detergents or aminoalcohols are included. Tissues treated with FRUIT and Sca*l*eS can be clearly stained with the lipid probe DiI (Hama et al. 2015, Hou et al. 2015). Taken together, the evidence suggests that urea may initiate the import of external small molecules into tissues by increases in osmotic pressure inside tissues without disturbing the lipid bilayer membrane and by relaxation and solvation of highly dense fiber proteins. The Mason group has developed a formamide-based clearing protocol termed *Clear*^{T} (Kuwajima et al. 2013). Formamide

is also a small, uncharged denaturant with both hydrogen donor and acceptor groups. However, the hydration energy of urea is expected to be much higher than that of formamide because of the strong synergetic effect of two NH_2 groups, according to a comparison between urea and the formamide derivative acetamide (Jedlovszky & Idrissi 2008). Actually, 10-wt% urea solution exhibited higher swelling ability and clearing performance for the adult mouse brain than did 10-wt% formamide solution (T. Murakami & H.R. Ueda, unpublished result). Nevertheless, *Clear^T* transparentized whole mice embryos much more rapidly and efficiently than did Sca*l*eA2. This is mainly because polar formamide considerably dehydrates tissues by serially increasing the concentration up to 95%. Formamide is an aprotic polar solvent like *N*,*N*-dimethylformamide and DMSO and can solubilize lipids. Therefore, delipidation of tissues by high concentrations of formamide may contribute to the clearing performance of *Clear^T*. Strictly speaking, formamide should be categorized as a water-miscible polar solvent. But we introduce this denaturant as a hydrogen-promoting solvent to compare it with urea.

Permeabilization by substitution of water with hyperhydration reagents driven by the osmotic pressure difference is a straightforward strategy for preservation of an intact hydration environment inside tissues. In the ancient past, people soaked fruits in syrup for antisepsis to create a translucent glaze. Analogously, the Imai group developed a fructose-based clearing method termed SeeDB (Ke et al. 2013). In this protocol, fixed tissues are serially incubated in 20% (wt/vol) to 80.2% or 86.7% (wt/wt) fructose solution. SeeDB-treated tissues kept their original sizes throughout the protocol. Osmotic dehydration was adequately balanced with permeation of the small monosaccharide fructose by controlling gradual increases in fructose concentration. However, the extremely high viscosity of the saturated fructose solution complicates preparation, handling, and cleanup.

To address this issue, the Jiang group developed less viscous cocktails containing fructose and urea, termed FRUIT (Hou et al. 2015). They also investigated osmotically balanced protocols without tissue deformation and demonstrated the importance of the gradient in solute concentration and the balance of ionic osmotic pressure. Nevertheless, fructose-based protocols such as SeeDB and FRUIT cannot avoid Maillard browning discoloration derived from the reactive ketone group of fructose, even in the presence of reductants such as α-thioglycerol.

The Miyawaki group established a new clearing protocol, Sca*l*eS, by combination of urea and the monosaccharide sorbitol, which lacks a ketone group (Hama et al. 2015). Sca*l*eS succeeds in the rapid clearing of brain tissues without significant deformation by means of the osmotically balanced potentiation of molecular flux across tissues. Importantly, clearing by Sca*l*eS is free from tissue discoloration, from quenching of the fluorescent reporter, and from loss of presynaptic and postsynaptic fabrics. The Miyawaki group also mentioned pretreatment with a cocktail containing 1 mM methyl β-cyclodextrin, 1 mM γ-cyclodextrin, and 1% *N*-acetyl-L-hydroxyproline; this cocktail enhanced tissue permeability. Both of these cyclodextrins are used for extraction of cholesterol from the plasma membrane (Kilsdonk et al. 1995), and *N*-acetyl-L-hydroxyproline loosens collagen structures (Hama et al. 2015). Therefore, removal of cholesterol and relaxation of collagen fibers may expedite molecular influx into tissues.

Delipidation Reagents

As described below, hydrophilic molecules suitable for RI-matching medium such as contrast materials do not tend to diffuse inside intact tissues due to their large molecular size. Thus, tissue delipidation is important for the full permeation of high-RI medium into deep regions of tissue. Among water-soluble molecules, detergents solubilize lipids efficiently. Our group attempted to develop a novel screening system to discover hydrophilic chemical candidates with high lipophilicity

in biological tissues (Susaki et al. 2014). We used PFA-fixed brain homogenate instead of a whole-brain sample for the screening so that many chemicals could be tested using only one mouse brain. The homogenate was mixed with 10 wt% of each chemical solution, and turbidity of the resulting mixture at OD600 (optical density measured at a wavelength of 600 nm) was recorded. The potential solubility of each chemical to brain lipids was expected to correlate with reduction of the turbidity of the homogenate. We screened 40 chemicals, including polyhydric alcohols, detergents, and hydrophilic small molecules, corresponding to the ingredients of the Sca*l*eA2 solution: glycerol, Triton X-100, and urea. Interestingly, a series of aminoalcohols are highly effective in solubilizing the homogenate compared with other alcohols. Taking into account clearing performance for hemisphere and quenching of fluorescent proteins, we finally arrived at a cocktail of 25-wt% Quadrol, 15-wt% Triton X-100, and 25-wt% urea, termed Sca*l*eCUBIC-1. Sca*l*eCUBIC-1 treatment efficiently extracted phospholipids and cholesterol from organ samples to result in highly cleared specimens after PBS washing and RI matching. Because the complete mixture had higher clearing ability than did each individual solution alone and every combinatorial solution of two of the three components, we concluded that each chemical works independently. Presumably, basic Quadrol solubilizes phospholipids by electrostatic interaction, whereas Triton X-100 incorporates lipids into a micelle. Urea may accelerate permeation of other ingredients by increasing internal osmotic pressure and/or may relax dense fiber proteins as described above. Recently, we developed an improved cocktail, Sca*l*eCUBIC-1A, to further preserve fluorescence of reporters. The composition of Sca*l*eCUBIC-1A is as follows: 5-wt% Quadrol, 10-wt% Triton X-100, 10-wt% urea, and 0–25 mM NaCl (Susaki & Ueda 2016; protocol available at **http://cubic.riken.jp**). In this new protocol, ionic osmolality by the addition of salt prevents excess sample swelling. We discovered the novel clearing ability of aminoalcohols, despite a relatively small chemical library. Further comprehensive screening should expand the number of hydrophilic reagents with high clearing performance and should reveal additional chemical principles for tissue clearing through detailed chemical profiling. Our chemical screening concept is also applicable to whole-plant clearing. On the basis of a similar combinatorial method, the Kurihara group developed an optical clearing cocktail, termed ClearSee (Kurihara et al. 2015), which efficiently elutes chlorophyll as a source of autofluorescence while maintaining fluorescent protein stability. In contrast to the Sca*l*e-based clearing cocktail by the Sherrier group (Warner et al. 2014), ClearSee succeeded in the considerable removal of chlorophyll inside plant tissue.

All CLARITY-relating clearing methods are based on delipidation by the ionic detergent SDS (**Figure 1**). Detergents very slowly penetrate into tissues, probably because of their large molecular size, as shown in passive CLARITY and PACT. Thus, acceleration of diffusion kinetics of detergents inside tissues is required to sufficiently achieve lipid removal in deep tissue. Therefore, increasing internal osmotic pressure by urea permeation is a feasible strategy, as in Sca*l*eCUBIC-1, to passively facilitate detergent influx. Alternatively, there are three other strategies for promoting diffusion of detergents: electric field potential, transcardial perfusion, and thermal energy.

Electric field potential is the most promising approach to reinforce diffusion of ionic detergents. The Deisseroth group first introduced the electrophoresis-based clearing method CLARITY to render rapid and full clearing of a whole mouse brain (Chung et al. 2013). In this protocol, hydrogel-embedded tissue samples were delipidated by active diffusion of SDS into tissues induced by an electric field potential. For proper tissue clearing, a homogeneous electric field and constant temperature and pH in the electric chamber should be maintained (Tomer et al. 2014). Because for this electrophoretic tissue clearing method there is much room for optimization of conditions such as electric potential, temperature, electrode, and chamber, many kinds of CLARITY-derived methods have been reported (Costantini et al. 2015, Epp et al. 2015, Kim et al. 2015, Lee et al. 2014, Palmer et al. 2015). High-voltage (>50-V) application in static one-directional electric field causes

significant tissue deformation, although diffusion of charged molecules is theoretically accelerated in proportion to voltages greater than 10 V. Increased diffusion may occur because application of such large electrical forces can also strain endogenous charged biomolecules such as DNA and proteins. Interestingly, the Chung group revealed that a rotational electric field selectively electrotransported charged molecules even under high-voltage application and therefore led to rapid tissue clearing without macroscopic and microscopic deformation (Kim et al. 2015). Although device design is complicated, this system represents the most rational and efficient electrophoretic clearing device.

In animals, blood is usually delivered to the body through the circulatory system by the heart pumping. Thus, transcardial perfusion is another strategy to enforce detergent permeation inside tissues. The Gradinaru group first introduced this type of clearing protocol, termed PARS (Yang et al. 2014). Whole-body clearing by continuous perfusion of SDS-based clearing medium provided fully transparentized whole-organ samples such as brain, heart, lung, liver, and kidney after RIMS treatment (Treweek et al. 2015). We have also developed another CUBIC protocol for the combination of simple immersion and temporal perfusion of half-diluted Sca*l*eCUBIC-1 (Tainaka et al. 2014). Both internal clearing by perfusion and external clearing by immersion allowed for further effective clearing of whole-body samples (Susaki et al. 2015). As a result, the CUBIC perfusion protocol has enabled whole-body and whole-organ imaging at the single-cell resolution by commercially available LSFM for the first time.

Because solute diffusion kinetics is dependent on temperature, thermal activation of diffusion appears to be a straightforward strategy (Murray et al. 2015). However, because PFA-fixed tissues would be damaged by a strong surfactant solution at elevated temperatures, passive clearing protocols are usually conducted below 37°C. In other words, the fixation intensity of tissues limits the thermal diffusion kinetics of detergents. As described above, the Chung group has introduced SWITCH-based glutaraldehyde fixation. Those highly fixed tissues are successfully resistant to boiling in SDS-based buffer, even at 80°C.

DECOLORIZING

To achieve whole-organ/whole-body clearing, it is important to decolorize endogenous pigments such as heme, riboflavin, melanin, and lipofuscin (Tuchin 2015). These pigments usually interfere with observation. Whereas heme and riboflavin are small ligands for endogenous proteins, melanin and lipofuscin are oxidatively polymerized pigments that are derived from the amino acid tyrosine (Sealy et al. 1980) and lipoproteins (Brizzee et al. 1984), respectively. Generally, those pigments can be readily bleached by several oxidative treatments (Andersen et al. 2012). In particular, H_2O_2, one of the most widely used bleaching chemicals, directly degrades the pigment structure (Dowson 1983, Li et al. 2006, Manicam et al. 2014). Among the recent 3D imaging protocols, in iDISCO such oxidative bleaching was applied to suppress autofluorescence inside tissues (Renier et al. 2014). In spite of versatile availability for pigment bleaching, such harsh oxidation may be fraught with undesired protein degradation, leading to loss of GFP signals and antigenicity (Alnuami et al. 2008, Steinke & Wolff 2001). Thus, a milder decoloration strategy is required for tissue clearing to establish multi-imaging systems compatible with small fluorescent probes, fluorescent proteins, and immunological labeling.

To visualize detailed structures in deeper organs, we must overcome light absorbance by heme, which is one of the most abundant chromophores in the body (Horecker 1943, Weissleder 2001). However, heme tightly binds to hemoglobin and can be released only in highly acidic (≤pH 2) or highly basic (≥pH 11) conditions (Kristinsson & Hultin 2004, Teale 1959). Recently, we discovered another unexpected chemical nature of aminoalcohols: tissue decolorization (Tainaka et al.

2014). Q bands (~500–700 nm) of heme in erythrocytes treated with Quadrol or Sca*l*eCUBIC-1 reagent were considerably changed from those of the hemoglobin-bound form. These results imply that aminoalcohols may be bound to heme porphyrin instead of oxygen and histidine in hemoglobin; this tendency to bind heme porphyrin may facilitate heme release and may explain the unexpected expansion of the effective pH window for heme release. Additionally, the buffering capability of Quadrol in moderately basic conditions should also contribute to the decolorizing performance. SDS-based CLARITY protocols also succeeded in decolorizing heme-rich organs (Epp et al. 2015, Lee et al. 2014, Treweek et al. 2015). This is probably because charged heme molecules could be eluted by electrophoretic force as well as by denaturation of the heme-hemoglobin holoenzyme by SDS.

Unlike the case of heme, there has been no feasible method for decolorizing large pigments such as melanin and lipofuscin, except for harsh bleaching. It is inherently difficult to elute such polymerized pigments without degradation of other constituents. Thus, we have to explore alternative strategies to address this issue. In the case of lipofuscin, its strong autofluorescence is the prominent obstacle for optically fluorescence imaging of elderly tissues. Copper(II) sulfate and Sudan Black B efficiently reduced lipofuscin autofluorescence without significant interference with other fluorophores in sectioned tissues (Schnell et al. 1999). The Gradinaru group demonstrated that Sudan Black B staining is successfully compatible with tissue clearing, fluorescent reporters, and immunostaining (Treweek et al. 2015). After whole-body clearing by CUBIC, pigments in eyeballs still impede light transmission due to the strong absorbance of light. Thus, decolorizing of melanin remains a challenge.

Several clearing protocols, such as fructose-based SeeDB and FRUIT and glutaraldehyde-based SWITCH, cause undesired Maillard-type discoloration of tissues (Hou et al. 2015, Ke et al. 2013, Murray et al. 2015). The reactive ketone of fructose or aldehyde of glutaraldehyde initially reacts with the nucleophilic amino group of endogenous constituents to form Schiff bases, followed by reversible Amadori rearrangement and irreversible polymerization (Leung 1987). The formation of the heterogeneous polymer melanodin may be facilitated at high temperatures and low water activity. This discoloration seriously interferes with light transmission. However, such discoloration can be partly suppressed by reduction by α-thioglycerol or sodium sulfite (Ke et al. 2013, Murray et al. 2015), possibly because the reductive amination of Schiff bases would deactivate the generation of highly reactive aldehyde intermediates to terminate the polymerization.

REFRACTIVE INDEX MATCHING

RI matching is a final step for tissue clearing to homogenize the RI of the entire tissue. Solutes and solvents bearing an aryl and/or iodo group display higher RI than do other solutes and solvents. Moreover, the RI of a solution increases depending on the solute concentration. Thus, high-RI media are generally composed of aromatic solvents or dense aqueous solutions containing highly water-soluble contrast reagents or polyalcohols like sugars. The optimum RI value for each biological tissue depends on the contents and densities of lipids, proteins, and other constituents (Johnsen & Widder 1999, Tuchin 2015). Although current protocols have been optimized for mice brains, RIs of the available media range from 1.44 to 1.56, as shown in **Table 1**. We discuss RI matching by comparing protocols to give useful chemical insight into the optimum RI value.

Both BABB and DBE are organic RI-matching media with the same RI value ($n = 1.56$). However, DBE has faster kinetics and higher potency in tissue clearing than does BABB (Becker et al. 2012). These differences may be attributed to a difference in viscosity (DBE viscosity = 5.3 cP; BABB viscosity = ~8.8 cP). THF-dehydrated tissues become rapidly transparentized after immersion in DBE. But cleared tissues become opaque again after prolonged incubation in DBE

without any change in sample size, indicating that the equilibrated RI value (near 1.56) does not exactly match with the RI of THF- and DBE-treated brains. Because it takes a long time to reach equilibrium in efflux of embedded THF while the influx kinetics of DBE balances with the efflux kinetics of THF, an optimum RI value for brain samples by the THF and DBE clearing is expected to be lower than 1.56.

Diatrizoic acid [FocusClear, $n = 1.46$ (Chiang 2002)], Histodenz [RIMS, $n = 1.47$ (Yang et al. 2014); SeeDB2, $n = 1.52$ (Ke et al. 2016)], and iodixanol [SWITCH-related RI medium, $n = 1.47$ (Murray et al. 2015)], which are known as contrast reagents, are utilized as hydrophilic RI media because of their extremely high solubility in water (**Figure 1**). However, contrast reagent–based RI media require intensive removal of the plasma membrane in the permeabilization step due to their large molecular size. Because CLARITY-related clearing protocols can achieve full delipidation of the tissues of interest by various kinds of permeabilization strategies, these RI media are suitable for such protocols. Among hydrophilic methods, these protocols provide the greater clearing of specimens. Thus, the optimum RI value of the lipid-removed brain samples is considered to be approximately 1.46–1.47 [the SeeDB2 cocktail was designed to match the refractive indices of immersion oil ($n = 1.518$)]. These reagents can also contribute to high-RI media, even in relatively high water content, in addition to modest viscosity. Therefore, these media avoid excess tissue shrinkage after equilibrium.

Polyalcohols such as glycerol ($n = 1.47$), fructose [SeeDB, $n = 1.49$ (Ke et al. 2013)], sucrose [Sca*l*eCUBIC-2, $n = 1.49$ (Susaki et al. 2014)], sorbitol [sRIMS, $n = 1.44$ (Yang et al. 2014); Sca*l*eS4, $n = 1.44$ (Hama et al. 2015)], and aprotic DMSO (Economo et al. 2016, Hama et al. 2015) are also highly soluble in water and are therefore suitable for preparation of high-RI media. These reagents have a significant cost advantage over contrast reagents, but sugar-based RI media are inferior in clearing performance. Small glycerol and monosaccharides are suitable for delipidation-free clearing methods such as Sca*l*e and SeeDB. Because these protocols cannot result in fully transparentized brain samples, the optimum RI value of lipid-intact brain tissues is still unclear. In the CUBIC protocol, the disaccharide sucrose accelerates permeation into lipid-removed tissues by increasing internal osmotic pressure. Additionally, urea osmotically counterbalances dehydration by sucrose to escape from both shrinking and swelling in a fashion similar to that of Sca*l*eS. CUBIC-treated brain samples are clear enough to be applied to LSFM. But the clearing efficiency of the CUBIC protocol is less than the clearing efficiencies of THF-DBE and CLARITY-related clearing protocols (Hama et al. 2015, Kim et al. 2015). The lower clearing efficiency of the CUBIC protocol is probably because lipids in the brain are not fully removed through this protocol. This may be why the CUBIC-optimized RI value ($n = 1.49$) needs to be slightly higher than the RI value of CLARITY-related protocols ($n = 1.46$–1.47).

PRESERVATION OF FLUORESCENT SIGNALS FROM REPORTER PROTEINS

Fluorescent proteins such as GFP from the jellyfish (Shimomura et al. 1962, Tsien 1998) are well-established and versatile reporter proteins for monitoring gene expression profiles (Chalfie et al. 1994), protein localization (Nienhaus & Nienhaus 2014), and sensing endogenous molecules (Mehta & Zhang 2011) in a variety of systems. The structure of the GFP chromophore was characterized as *p*-hydroxybenzylideneimidazolinone (Cody et al. 1993, Shimomura 1979), which is formed by internal cyclization of a Ser-Tyr-Gly tripeptide and 1,2-dehydrogenation of the Tyr (Cubitt et al. 1995). Wild-type GFP displays a pronounced bimodal absorption profile with two peaks at approximately 400 and 470 nm, corresponding to the protonated and the deprotonated forms of the chromophore, respectively (Brejc et al. 1997, Dong et al. 2006). Therefore, the

protonation state of the chromophore strongly affects fluorescent emission from 488-nm excitation. Most fluorescent proteins, including Venus (Rekas et al. 2002), mFruits (Shu et al. 2006), mKate (Pletnev et al. 2008), and DsRed (Yarbrough et al. 2001), share similar chromophore structures, and the deprotonated phenolate forms usually exhibit strong fluorescent emission excited by the desired wavelengths (Ormö et al. 1996). Thus, fluorescence highly depends on pH (Kneen et al. 1998) and ionic strength (Ward et al. 1982). Also, the organic solvents (Hama et al. 2011), detergents, and chaotropic denaturants (Stepanenko et al. 2012) used in the clearing protocols potentially suppress fluorescent signals from GFP derivatives by protein denaturation. We have to keep in mind the two deactivation mechanisms of GFP derivatives: (*a*) protonation of the chromophore and (*b*) denaturation of the protein structure.

Generally, GFP signals are attenuated by dehydration processes such as EtOH-BABB, relatively GFP-friendly THF-DBE, TDE, and *Clear*^{T}. Even fructose-based SeeDB also somewhat suppresses GFP fluorescence, possibly due to low water content (Hama et al. 2015). It is inevitable that dehydration progressively denatures GFP and results in the decay of GFP fluorescence. However, suppressed EGFP fluorescence in resin-embedded dehydrated tissues was dramatically recovered by alkaline buffer solution treatment (Xiong et al. 2014). Also, the Giese group demonstrated that EGFP signals were sufficiently preserved through dehydration by pH-adjusted 1-PrOH or *t*-BuOH and remained for more than 100 days in BABB solution at 4°C (Schwarz et al. 2015). For the preservation of GFP signals, it is important to maintain a basic-pH condition, with pH adjusted to 9.5 with nonionic trimethylamine. Thus, fluorescent suppression by the protonation of the chromophore is prior to irreversible quenching by protein denaturation, and denaturation can be dramatically reduced, even in organic solvents. Unlike 1-PrOH and *t*-BuOH, MeOH and EtOH failed to preserve GFP fluorescence by the same pH adjustment. A small MeOH or EtOH may penetrate the barrel structure to inhibit the deprotonation of the chromophore. These results indicate that GFP signals can be sufficiently preserved through the previously reported dehydration protocols by appropriate pH control.

In contrast, GFP fluorescence is considered to be quenched by protein denaturation in detergent-based protocols such as CLARITY-related methods, PACT-PARS, and CUBIC. The quenching of GFP is also significantly affected by temperature (dos Santos 2012, Schwarz et al. 2015). Incubation at elevated temperature may denature GFP proteins while promoting tissue clearing. GFP fluorescence is well preserved between pH 7.0 and 11.5 at room temperature but is well preserved only at ~pH 7.5 at 45°C (T. Murakami & H.R. Ueda, unpublished result). Sca*l*eCUBIC-1 is too basic to preserve GFP signals under long incubation times at 37°C. The composition of Sca*l*eCUBIC-1A was modified to avoid quenching of GFP signals without disturbing clearing performance (Susaki & Ueda 2016; for more details, please see **http://cubic.riken.jp**).

Among the clearing protocols, urea/sorbitol-based Sca*l*eS is the best protocol for ensuring GFP fluorescence (Hama et al. 2015). Although this cocktail contains high concentrations of urea, permeated urea is not sufficient to denature GFP proteins.

STAINING OF ENDOGENOUS COMPONENTS

Recent advances in tissue-clearing techniques allowed us to visualize entire organs at single-cell resolution. Early work relating to 3D tissue imaging have mainly used reporter mice expressing exogenous fluorescent proteins. Reporter mice are particularly suitable for these technologies because organ samples could be visualized by microscopes just after tissue clearing. However, reporter animals are limited to certain strains and species. Thus, researchers have also intensively tackled tissue-staining methods by fluorescent dyes and antibodies to label specific and various molecular markers as listed in **Table 2**. Unfortunately, these molecules permeate very slowly

Table 2 Tissue-staining protocols

Reference	Protocol	Sample	Staining procedure	Fluorescent dye	Application
Ertürk et al. 2012	3DISCO	Mouse: brain, spinal cord, lung, mammary glands, spleen, lymph node	Diffusion-limited staining	Cy3 anti-smooth muscle actin, FITC lectin, Alexa Fluor 488	Vasculature, tumor cells, and immune cells
Renier et al. 2014	iDISCO (3DISCO clearing)	Mouse: brain, kidney, embryonic head, embryonic spinal cord	Diffusion-limited staining, antibody penetration driven by dehydration-rehydration process by MeOH and PBS	TO-PRO family, EdU labeling, CTB	Neuroanatomy; neuronal pathophysiology; and neural development, activity, and degradation
Kuwajima et al. 2013	*Clear*^{T}, *Clear*^{T2}	Mouse embryo	Diffusion-limited staining	DiI, CTB, Hoechst	Neural tracing
Hama et al. 2011, 2015	Sca*l*e, Sca*l*eS	Mouse: brain, embryonic brain; human: brain	Diffusion-limited staining; urea induces molecular flux	DiI, PP-BTA-1, PI	Vasculature, development, connectomics, and plaque pathogenesis in Alzheimer's disease
Ke et al. 2013	SeeDB	Mouse: brain, embryo	Diffusion-limited staining	DiI	Neural tracing and anatomy
Susaki et al. 2014, 2015; Tainaka et al. 2014	CUBIC	Mouse: brain, heart, lung, kidney, liver, spleen, pancreas, intestine, stomach, muscle, skin, ear, whole body; marmoset: brain	Diffusion-limited staining	PI, SYTO 16	Neural activity, anatomy, and pathology
Chung et al. 2013, Costantini et al. 2015, Epp et al. 2015, Lee et al. 2014, Tomer et al. 2014	CLARITY	Mouse: brain, pancreas, liver, kidney, lung, intestine, spleen, muscle, testis; human: brain	Diffusion-limited staining	DAPI, PI, SYTO 16	Neural anatomy and pathology, in situ hybridization, multiple rounds of staining and destaining
Treweek et al. 2015, Yang et al. 2014	PACT-PARS	Mouse: brain, heart, lung, kidney, liver, spinal cord, pancreas, intestine, tibia, spleen, adrenal gland, fallopian tube, ovary, whole body; rat: brain, spinal cord; human: tumor biopsy, pancreas	PACT: diffusion-limited staining; PARS: staining by transcardial perfusion	DAPI, Hoechst, SYTO 24, DRAQ5, acridine orange/methylene blue, NeuroTrace™ 530/615 red fluorescent, DyLight 488 lectin, Atto 565–phalloidin, Alexa Fluor 647 phalloidin	Anatomy, tumor cells, and pathology; in situ hybridization

(*Continued*)

Table 2 (*Continued*)

Reference	Protocol	Sample	Staining procedure	Fluorescent dye	Application
Kim et al. 2015	Stochastic electrotransport	Mouse: brain, heart, lung, kidney, liver, intestine	Staining by stochastic electrotransport	TO-PRO-3, SYTO 16, Dylight 594 tomato lectin	Vasculature and neuroanatomy
Lee et al. 2016	ACT-PRESTO (CLARITY-based clearing)	Mouse: brain, lung, kidney, liver, spleen, intestine, testis, thymus, whole body; rat: brain, embryo; zebrafish: whole body; rabbit: brain; human: spinal cord	Staining by centrifugal force (*c*-PRESTO) or convection flow (*s*-PRESTO)	DAPI, SYTO 16	Neural tracing, in situ hybridization
Murray et al. 2015	SWITCH	Mouse: brain, heart, lung, kidney, spinal cord; rat: brain, spinal cord; marmoset: brain; human: brain	Diffusion-limited staining controlled by the interaction between dyes and their targets	DAPI, DiD, DyLight 488 lectin	Entire myelinated fiber tracts in mouse brain, in situ hybridization, multiple rounds of staining and destaining

through a tissue matrix entangled with fibrous proteins and other constituents, and it usually takes a long time to stain thick tissues (over approximately the millimeter scale) uniformly (Kim et al. 2015). To address this issue, we have to gain deeper insight into the principles of permeation kinetics of external molecules. In this section, we highlight current staining protocols optimized for individual clearing protocols and discuss key features of permeation kinetics.

Generally, the staining kinetics of fluorescent molecules depends on the diffusion kinetics and the chemical interactions with endogenous molecules. The diffusion kinetics in the tissue matrix may be highly affected by the degree of fixation, probably because the degree of fixation would determine the pore size of polymerized protein networks inside the tissue (Yang et al. 2014). Thus, ensuring sufficient pore size is important so that dyes can spatially pass through tissues. Because the cell membrane strictly limits molecular flux, permeabilization would also critically promote the access of dyes to intracellular biomolecules. Dyes that have permeated into the tissue are surrounded by enormous endogenous molecules. The diffusion of dyes could be substantially retarded by interactions with such molecules. Therefore, temporal cancellation of those interactions could dramatically accelerate diffusion into deeper regions. A careful review of current protocols, including iDISCO, CUBIC, Sca*l*eS, and SWITCH, as well as CLARITY-related protocols, would shed light on the underlying principles of chemical staining.

iDISCO

iDISCO is a rapid staining protocol that uses organic solvents in combination with 3DISCO by the Tessier-Lavigne group (Renier et al. 2014). A dehydration-rehydration process by MeOH and PBS significantly facilitated antibody penetration into the sample, but the mechanism by which this occurred was not clear. Perhaps the hydrophobic denaturation process loosened polymerized protein matrices to expand pore size. In any case, the iDISCO technique allowed for whole-mount labeling of embryo mice and several adult mice organs and was compatible with 28 antibodies and

several fluorescent dyes. Adult mice brains were stained to visualize the projections of dopaminergic neurons and axons of sensory neurons. In addition to neuroanatomy, Renier et al. used iDISCO for neuronal pathophysiology, including neural development, activity, and degradation. Unfortunately, 3DISCO-based clearing seems to be unable to decolorize blood-infused tissues, because significant autofluorescence remains after the process is complete. Renier et al. suggest peroxide bleaching to overcome this problem, but this treatment may result in loss of antigenicity and in protein destruction. Currently, longer excitation/emission wavelengths, especially in the far-red region, are needed for iDISCO images with high signal-to-noise ratio. Because iDISCO is incompatible with many fluorescent reporters, Renier et al. suggest antibody labeling of each fluorescent protein. However, passive antibody labeling appears to be too slow to stain whole adult mice bodies homogeneously, so techniques that can utilize fluorescent proteins without antibody staining are more attractive for WBC profiling.

CUBIC

In the CUBIC protocol, Sca*l*eCUBIC-1 efficiently removes lipids from conventional PFA-fixed tissues. Thus, exogenous molecules easily permeate into cells. CUBIC enabled homogeneous whole-mount staining of millimeter- to centimeter-sized samples, including major organs of adult mice, primate brains, and whole mice bodies, by several nuclear staining dyes (Susaki et al. 2014, Tainaka et al. 2014). Nuclear counterstaining is necessary to acquire whole-organ structural images, which can be used for anatomical annotation in computational comparative analyses. Neural activities of Arc-dVenus transgenic mice induced by environmental stimulation were also quantified at single-cell resolution. In addition, a comprehensive and statistical analysis of Langerhans islets (LIs) in the diabetic pancreas revealed that larger LIs are more sensitive to β cell impairment. CUBIC was also applicable to whole-mount immunolabeling of several organs such as the heart, lung, stomach, and intestine under a conventional PBST (2% Triton X-100 in PBS)-based staining condition. The low concentration of the detergent may contribute to increased permeation kinetics by the disruption of interactions between antibody and endogenous biomolecules in spite of potential denaturation. However, CUBIC has relatively lengthy protocols in clearing and staining. The tested antibodies are also limited. These issues will be overcome largely by the exploration of further effective clearing chemicals and by optimization of permeation kinetics of labeled molecules.

Sca*l*eS

Sca*l*eS can clear tissue by urea-driven molecular flux tissue without significant disturbance of the plasma membrane (Hama et al. 2015). Thus, urea seems to be necessary for fluorescent molecule penetration into cells. Hama et al. (2015) established AbSca*l*e and ChemSca*l*e protocols for antibody and fluorescent dye staining, respectively. Both protocols relied on urea-based staining solution, but AbSca*l*e used a more modest urea concentration to avoid antibody denaturation. Urea and *N*-acetyl-L-hydroxyproline also solvate collagen fibers to relax entangled protein networks. These chemical treatments may play a role in the effective permeation of outer molecules by enlargement of inside pores. Hama et al. also conducted 3D imaging in a mouse model of Alzheimer's disease (AD) to establish proof of concept of chemical staining. They observed amyloid β (Aβ) plaques with both the anti-Aβ antibody and the fluorescent probe and evaluated inflammatory response in an AD mouse brain by double staining of Aβ plaques and microglia. Although whether AbSca*l*e is adaptable to a wide variety of antibodies is unclear, the series of chemical treatments in Sca*l*e appears to be the most likely to preserve intact structures among the currently available protocols.

CLARITY-Related Protocols

The original CLARITY protocol transparentized whole adult brains by electrophoretic delipidation (Chung et al. 2013). Permeabilized brain samples permitted the penetration of various kinds of antibodies, dye molecules, and even 50-base-pair RNA probes by passive diffusion. Interestingly, immunolabeling of hydrogel-embedded tissues can be recycled by denaturation by ionic detergents without fine structural damage or degraded antigenicity. This staining strategy was also applied to extensively fixed human tissues to visualize and identify neurons and projections. Hydrogel embedding significantly increased preservation of endogenous proteins during the detergent-based clearing step. But strong fixation also caused high cross-link density in the acrylamide polymer and inhibited the diffusion kinetics of exogenous molecules. The Gradinaru group optimized the contents of the fixative to accelerate passive diffusion of exogenous molecules (Yang et al. 2014). This group's continuous perfusion-based PARS protocol mimicks a heart pumping blood and significantly facilitates the permeation of dye molecules into deep tissue through the vascular system. This protocol also enables staining of antibodies, fluorescent probes, and RNA probes to various organs, including the brain, heart, lung, liver, and kidney, and has advanced our chemical understanding of tissue clearing and staining (Treweek et al. 2015). However, staining by passive diffusion may be too slow to label large organ samples homogeneously. The Chung group proposed an alternative rapid staining strategy based on stochastic electrotransport (Kim et al. 2015). A rotational electric field selectively dispersed highly electromobile molecules without interfering with the endogenous biomolecules. Significantly, all four molecules, even though they had different molecular sizes (70 to 2,000 kDa), benefitted from stochastic electrotransport in their electromobility. This strategy achieved homogeneous staining of whole-organ samples by fluorescent dyes, proteins, and antibodies within 1 day. More recently, the Sun group reported another staining strategy, termed ACT-PRESTO (active clarity technique–pressure-related efficient and stable transfer of macromolecules into organs) (Lee et al. 2016). Centrifugal force (*c*-PRESTO) or convection flow (*s*-PRESTO) enabled rapid immunostaining in 100-μm-thick sections within 2–3 h, whereas free diffusion requires 1–2 days. Although Lee et al. (2016) mainly combined their method with CLARITY, the concept could be applicable to other staining methods.

SWITCH

The principle of column chromatography is helpful for understanding the diffusion kinetics of dyes into tissue matrices. The mobility of an analyte on a column is determined by the affinity of the analyte to the stationary phase under the eluent. The analyte flows through the column in an elute buffer but remains on the column in binding buffer. The Chung group established a rapid chemical staining concept termed SWITCH (Murray et al. 2015). Dyes first penetrate into tissues in the SWITCH-OFF solution, which interrupts the interaction between the dyes and their target. Then the dyes specifically bind to their target after replacement of the SWITCH-OFF solution with a SWITCH-ON solution, which enhances the interaction between the dyes and their target. This technique enables uniform staining of a lipid probe (DiI) and antibodies, even in glutaraldehyde-fixed brain tissues. Because only 1-mm-thick slices of mice brains were immunolabeled in the Murray et al. (2015) study, it is unclear whether this protocol will be applicable to larger tissues. Pores in glutaraldehyde-fixed tissue matrices may be relatively small for antibody penetration. Nevertheless, SWITCH is an important milestone in passive staining because this method revealed a chemical principle for molecular diffusion into the tissue matrix.

OUTLOOK

The growing development of tissue clearing/staining techniques—from the concept of tissue clearing proposed by Spalteholz 100 years ago to the rapid development of numerous techniques over the past decade—has increased our understanding of various biological events in different organs. In the future, technical challenges might focus on clearing entire rodent bodies or primate organs. The understanding of the chemical principles of tissue clearing/staining will accelerate WBC profiling, which will enable identification of cellular circuits across multiple organs and allow for analysis of cellular dynamics in stochastic and proliferative cellular processes. The journey into the inner space of mammalian body may result in amazing insights into the fundamental question of what is health.

FUTURE ISSUES

1. Alternative fixation methods capable of preserving proteins without dense packing of tissue matrix will offer the considerable benefits of compatibility of high clearing performance, prevention of quenching of fluorescent proteins, and permeability of staining molecules.
2. Comprehensive chemical profiling for tissue clearing will elucidate the chemical properties necessary for delipidation, decolorizing, RI matching, and other potential factors.
3. Although gel-based feeding of mice improves gastrointestinal interference with light transmission, these methods are inappropriate for long-term breeding. Nutritious feeds compatible with tissue clearing will facilitate whole-abdominal imaging.
4. PACT-deCAL and EtOH-BABB were used to successfully clear dissected bone tissues. More refined protocols that enable both delipidation and decalcification will enable visualization of the whole cardiovascular system and entire neural networks.
5. The skin could be transparentized by several clearing protocols. But skin substantially blocks permeation of media and disrupts clearing of inner tissues. Skin-permeable clearing reagents are needed to achieve whole-body imaging of the entire animal body.
6. Mild decolorizing chemistry will be required for highly polymerized melanin pigments in the skin, eyeball, hair, and some tumor cells without destruction of other endogenous constituents.
7. For high-throughput or large screening, it will be necessary to develop cost-effective labeling technologies that enable homogeneous whole-body staining with fluorescent dyes, fluorescently labeled antibodies, and nucleic acid probes.

DISCLOSURE STATEMENT

RIKEN has filed a provisional patent application based on the CUBIC works.

ACKNOWLEDGMENTS

We thank the lab members at the University of Tokyo, E.A. Susaki, and A. Millius for their kind help in preparing this article. This work was supported by the Program for the Brain Mapping by Integrated Neurotechnologies for Disease Studies from the Ministry of Education, Culture, Sports, Science and Technology (MEXT) of Japan; by the Program for the Basic Science and

Platform Technology Program for Innovative Biological Medicine from MEXT; by the Program for the AMED (Japan Agency for Medical Research and Development)-CREST (Core Research for Evolutional Science and Technology) from MEXT; by a Grant-in-Aid for Scientific Research (grant 25221004) from Japan Society for the Promotion of Science (JSPS); by a Grant-in-Aid for Scientific Research on Innovative Areas (grant 23115006) from JSPS; by strategic programs for R&D (President's discretionary fund) of RIKEN; by an intramural Grant-in-Aid from RIKEN Quantitative Biology Center; and by the Tokyo Society of Medical Science.

LITERATURE CITED

Alnuami AA, Zeedi B, Qadri SM, Ashraf SS. 2008. Oxyradical-induced GFP damage and loss of fluorescence. *Int. J. Biol. Macromol.* 43:182–86

Amat F, Hockendorf B, Wan Y, Lemon WC, McDole K, Keller PJ. 2015. Efficient processing and analysis of large-scale light-sheet microscopy data. *Nat. Protoc.* 10:1679–96

Amat F, Lemon W, Mossing DP, McDole K, Wan Y, et al. 2014. Fast, accurate reconstruction of cell lineages from large-scale fluorescence microscopy data. *Nat. Methods* 11:951–58

Andersen AP, Hasselager E, Hoyer P-E, Moller M, Prento P, et al. 2012. *Theory and Strategy in Histochemistry: A Guide to the Selection and Understanding of Techniques*. Berlin: Springer Science & Business Media

Aoyagi Y, Kawakami R, Osanai H, Hibi T, Nemoto T. 2015. A rapid optical clearing protocol using 2,2′-thiodiethanol for microscopic observation of fixed mouse brain. *PLOS ONE* 10:e0116280

Barton KN, Buhr MM, Ballantyne JS. 1999. Effects of urea and trimethylamine *N*-oxide on fluidity of liposomes and membranes of an elasmobranch. *Am. J. Physiol. Regul. Integr. Comp. Physiol.* 276:R397–406

Becker K, Jährling N, Saghafi S, Weiler R, Dodt HU. 2012. Chemical clearing and dehydration of GFP expressing mouse brains. *PLOS ONE* 7:e33916

Bentley MV, Kedor E, Vianna RF, Collett JH. 1997. The influence of lecithin and urea on the in vitro permeation of hydrocortisone acetate through skin from hairless mouse. *Int. J. Pharm.* 146:255–62

Bouxsein ML, Boyd SK, Christiansen BA, Guldberg RE, Jepsen KJ, Muller R. 2010. Guidelines for assessment of bone microstructure in rodents using micro-computed tomography. *J. Bone Miner. Res.* 25:1468–86

Brejc K, Sixma TK, Kitts PA, Kain SR, Tsien RY, et al. 1997. Structural basis for dual excitation and photoisomerization of the *Aequorea victoria* green fluorescent protein. *PNAS* 94:2306–11

Brizzee KR, Eddy DE, Harman D, Ordy JM. 1984. Free radical theory of aging: effect of dietary lipids on lipofuscin accumulation in the hippocampus of rats. *AGE* 7:9–15

Chalfie M, Tu Y, Euskirchen G, Ward WW, Prasher DC. 1994. Green fluorescent protein as a marker for gene expression. *Science* 263:802–5

Chen F, Tillberg PW, Boyden ES. 2015. Expansion microscopy. *Science* 347:543–48

Chhetri RK, Amat F, Wan Y, Hockendorf B, Lemon WC, Keller PJ. 2015. Whole-animal functional and developmental imaging with isotropic spatial resolution. *Nat. Methods* 12:1171–78

Chiang AS, Lin WY, Liu HP, Pszczolkowski MA, Fu TF, et al. 2002. Insect NMDA receptors mediate juvenile hormone biosynthesis. *PNAS* 99:37–42

Chung K, Deisseroth K. 2013. CLARITY for mapping the nervous system. *Nat. Methods* 10:508–13

Chung K, Wallace J, Kim SY, Kalyanasundaram S, Andalman AS, et al. 2013. Structural and molecular interrogation of intact biological systems. *Nature* 497:332–37

Cody CW, Prasher DC, Westler WM, Prendergast FG, Ward WW. 1993. Chemical structure of the hexapeptide chromophore of the *Aequorea* green-fluorescent protein. *Biochemistry* 32:1212–18

Costantini I, Ghobril JP, Di Giovanna AP, Mascaro AL, Silvestri L, et al. 2015. A versatile clearing agent for multi-modal brain imaging. *Sci. Rep.* 5:9808

Cubitt AB, Heim R, Adams SR, Boyd AE, Gross LA, Tsien RY. 1995. Understanding, improving and using green fluorescent proteins. *Trends Biochem. Sci.* 20:448–55

Díaz RS, Monreal J, Regueiro P, Lucas M. 1992. Preparation of a protein-free total brain white matter lipid fraction: characterization of liposomes. *J. Neurosci. Res.* 31:136–45

Dodt HU, Leischner U, Schierloh A, Jährling N, Mauch CP, et al. 2007. Ultramicroscopy: three-dimensional visualization of neuronal networks in the whole mouse brain. *Nat. Methods* 4:331–36

Dong J, Solntsev KM, Tolbert LM. 2006. Solvatochromism of the green fluorescence protein chromophore and its derivatives. *J. Am. Chem. Soc.* 128:12038–39

dos Santos AM. 2012. Thermal effect on *Aequorea* green fluorescent protein anionic and neutral chromophore forms fluorescence. *J. Fluoresc.* 22:151–54

Dowson J. 1983. A comparison of autofluorescence emission spectra of bleached neuromelanin in non-diseased substantia nigra with spectra of other intraneuronal pigments in non-diseased and diseased tissue. *Acta Neuropathol.* 61:196–200

Economo MN, Clack NG, Lavis LD, Gerfen CR, Svoboda K, et al. 2016. A platform for brain-wide imaging and reconstruction of individual neurons. *eLife* 5:e10566

Epp JR, Niibori Y, Liz Hsiang HL, Mercaldo V, Deisseroth K, et al. 2015. Optimization of CLARITY for clearing whole-brain and other intact organs. *eNeuro* 2; doi: 10.1523/ENEURO.0022-15.2015

Ertürk A, Becker K, Jährling N, Mauch CP, Hojer CD, et al. 2012. Three-dimensional imaging of solvent-cleared organs using 3DISCO. *Nat. Protoc.* 7:1983–95

Feng Y, Yu ZW, Quinn PJ. 2002. Effect of urea, dimethylurea, and tetramethylurea on the phase behavior of dioleoylphosphatidylethanolamine. *Chem. Phys. Lipids* 114:149–57

Greene RF Jr., Pace CN. 1974. Urea and guanidine hydrochloride denaturation of ribonuclease, lysozyme, alpha-chymotrypsin, and beta-lactoglobulin. *J. Biol. Chem.* 249:5388–93

Hama H, Hioki H, Namiki K, Hoshida T, Kurokawa H, et al. 2015. Sca*l*eS: an optical clearing palette for biological imaging. *Nat. Neurosci.* 18:1518–29

Hama H, Kurokawa H, Kawano H, Ando R, Shimogori T, et al. 2011. Sca*l*e: a chemical approach for fluorescence imaging and reconstruction of transparent mouse brain. *Nat. Neurosci.* 14:1481–88

Helander KG. 1994. Kinetic studies of formaldehyde binding in tissue. *Biotech. Histochem.* 69:177–79

Hirashima T, Adachi T. 2015. Procedures for the quantification of whole-tissue immunofluorescence images obtained at single-cell resolution during murine tubular organ development. *PLOS ONE* 10:e0135343

Hopwood D. 1967. Some aspects of fixation with glutaraldehyde. A biochemical and histochemical comparison of the effects of formaldehyde and glutaraldehyde fixation on various enzymes and glycogen, with a note on penetration of glutaraldehyde into liver. *J. Anat.* 101:83–92

Hopwood D. 1972. Theoretical and practical aspects of glutaraldehyde fixation. *Histochem. J.* 4:267–303

Horecker BL. 1943. The absorption spectra of hemoglobin and its derivatives in the visible and near infra-red regions. *J. Biol. Chem.* 148:173–83

Hou B, Zhang D, Zhao S, Wei M, Yang Z, et al. 2015. Scalable and DiI-compatible optical clearance of the mammalian brain. *Front. Neuroanat.* 9:19

Hua L, Zhou R, Thirumalai D, Berne BJ. 2008. Urea denaturation by stronger dispersion interactions with proteins than water implies a 2-stage unfolding. *PNAS* 105:16928–33

Isosaka T, Matsuo T, Yamaguchi T, Funabiki K, Nakanishi S, et al. 2015. Htr2a-expressing cells in the central amygdala control the hierarchy between innate and learned fear. *Cell* 163:1153–64

Jedlovszky P, Idrissi A. 2008. Hydration free energy difference of acetone, acetamide, and urea. *J. Chem. Phys.* 129:164501

Johnsen S, Widder EA. 1999. The physical basis of transparency in biological tissue: ultrastructure and the minimization of light scattering. *J. Theor. Biol.* 199:181–98

Ke MT, Fujimoto S, Imai T. 2013. SeeDB: a simple and morphology-preserving optical clearing agent for neuronal circuit reconstruction. *Nat. Neurosci.* 16:1154–61

Ke MT, Nakai Y, Fujimoto S, Takayama R, Yoshida S, et al. 2016. Super-resolution mapping of neuronal circuitry with an index-optimized clearing agent. *Cell Rep.* 14:2718–32

Keller PJ, Ahrens MB. 2015. Visualizing whole-brain activity and development at the single-cell level using light-sheet microscopy. *Neuron* 85:462–83

Keller PJ, Ahrens MB, Freeman J. 2015. Light-sheet imaging for systems neuroscience. *Nat. Methods* 12:27–29

Kilsdonk EP, Yancey PG, Stoudt GW, Bangerter FW, Johnson WJ, et al. 1995. Cellular cholesterol efflux mediated by cyclodextrins. *J. Biol. Chem.* 270:17250–56

Kim SY, Cho JH, Murray E, Bakh N, Choi H, et al. 2015. Stochastic electrotransport selectively enhances the transport of highly electromobile molecules. *PNAS* 112:E6274–83

Kneen M, Farinas J, Li YX, Verkman AS. 1998. Green fluorescent protein as a noninvasive intracellular pH indicator. *Biophys. J.* 74:1591–99

Kristinsson HG, Hultin HO. 2004. Changes in trout hemoglobin conformations and solubility after exposure to acid and alkali pH. *J. Agric. Food Chem.* 52:3633–43

Kurihara D, Mizuta Y, Sato Y, Higashiyama T. 2015. ClearSee: a rapid optical clearing reagent for whole-plant fluorescence imaging. *Development* 142:4168–79

Kuwajima T, Sitko AA, Bhansali P, Jurgens C, Guido W, Mason C. 2013. *Clear^T*: a detergent- and solvent-free clearing method for neuronal and non-neuronal tissue. *Development* 140:1364–68

Leblond F, Davis SC, Valdes PA, Pogue BW. 2010. Pre-clinical whole-body fluorescence imaging: review of instruments, methods and applications. *J. Photochem. Photobiol. B Biol.* 98:77–94

Lee E, Choi J, Jo Y, Kim JY, Jang YJ, et al. 2016. ACT-PRESTO: rapid and consistent tissue clearing and labeling method for 3-dimensional (3D) imaging. *Sci. Rep.* 6:18631

Lee H, Park JH, Seo I, Park SH, Kim S. 2014. Improved application of the electrophoretic tissue clearing technology, CLARITY, to intact solid organs including brain, pancreas, liver, kidney, lung, and intestine. *BMC Dev. Biol.* 14:48

Leung H. 1987. Influence of water activity on chemical reactivity. In *Water Activity: Theory and Applications to Food*, ed. LB Rockland, LR Beuchat, Inst. Food Technol., Int. Union Food Sci. Technol., pp. 27–54. New York: Marcel Dekker

Li D, Zhang X, Loni Y, Sunz X. 2006. Inactivation of hemoglobin by hydrogen peroxide and protection by a reductant substrate. *Life Sci. J.* 3:52–58

Liu H, Beauvoit B, Kimura M, Chance B. 1996. Dependence of tissue optical properties on solute-induced changes in refractive index and osmolarity. *J. Biomed. Opt.* 1:200–11

Manicam C, Pitz S, Brochhausen C, Grus FH, Pfeiffer N, Gericke A. 2014. Effective melanin depigmentation of human and murine ocular tissues: an improved method for paraffin and frozen sections. *PLOS ONE* 9:e102512

Mehta S, Zhang J. 2011. Reporting from the field: genetically encoded fluorescent reporters uncover signaling dynamics in living biological systems. *Annu. Rev. Biochem.* 80:375–401

Metz B, Kersten GF, Baart GJ, de Jong A, Meiring H, et al. 2006. Identification of formaldehyde-induced modifications in proteins: reactions with insulin. *Bioconjug. Chem.* 17:815–22

Metz B, Kersten GF, Hoogerhout P, Brugghe HF, Timmermans HA, et al. 2004. Identification of formaldehyde-induced modifications in proteins: reactions with model peptides. *J. Biol. Chem.* 279:6235–43

Murray E, Cho JH, Goodwin D, Ku T, Swaney J, et al. 2015. Simple, scalable proteomic imaging for high-dimensional profiling of intact systems. *Cell* 163:1500–14

Nienhaus K, Nienhaus GU. 2014. Fluorescent proteins for live-cell imaging with super-resolution. *Chem. Soc. Rev.* 43:1088–106

Ntziachristos V. 2010. Going deeper than microscopy: the optical imaging frontier in biology. *Nat. Methods* 7:603–14

Ode KL, Ueda HR. 2015. Seeing the forest and trees: whole-body and whole-brain imaging for circadian biology. *Diabetes Obes. Metab.* 17(Suppl. 1):47–54

Ogawa S, Lee TM, Nayak AS, Glynn P. 1990. Oxygenation-sensitive contrast in magnetic resonance image of rodent brain at high magnetic fields. *Magn. Reson. Med.* 14:68–78

Oh SW, Harris JA, Ng L, Winslow B, Cain N, et al. 2014. A mesoscale connectome of the mouse brain. *Nature* 508:207–14

Ormö M, Cubitt AB, Kallio K, Gross LA, Tsien RY, Remington SJ. 1996. Crystal structure of the *Aequorea victoria* green fluorescent protein. *Science* 273:1392–95

Pal SK, Peon J, Zewail AH. 2002. Biological water at the protein surface: dynamical solvation probed directly with femtosecond resolution. *PNAS* 99:1763–68

Pallotto M, Watkins PV, Fubara B, Singer JH, Briggman KL. 2015. Extracellular space preservation aids the connectomic analysis of neural circuits. *eLife* 4:e08206

Palmer WM, Martin AP, Flynn JR, Reed SL, White RG, et al. 2015. PEA-CLARITY: 3D molecular imaging of whole plant organs. *Sci. Rep.* 5:13492

Petty HR. 1993. *Molecular Biology of Membranes: Structure and Function*. Berlin: Springer Science & Business Media

Pletnev S, Shcherbo D, Chudakov DM, Pletneva N, Merzlyak EM, et al. 2008. A crystallographic study of bright far-red fluorescent protein mKate reveals pH-induced *cis-trans* isomerization of the chromophore. *J. Biol. Chem.* 283:28980–87

Priyakumar UD, Hyeon C, Thirumalai D, Mackerell AD Jr. 2009. Urea destabilizes RNA by forming stacking interactions and multiple hydrogen bonds with nucleic acid bases. *J. Am. Chem. Soc.* 131:17759–61

Ragan T, Kadiri LR, Venkataraju KU, Bahlmann K, Sutin J, et al. 2012. Serial two-photon tomography for automated ex vivo mouse brain imaging. *Nat. Methods* 9:255–58

Rekas A, Alattia JR, Nagai T, Miyawaki A, Ikura M. 2002. Crystal structure of Venus, a yellow fluorescent protein with improved maturation and reduced environmental sensitivity. *J. Biol. Chem.* 277:50573–78

Renier N, Wu Z, Simon DJ, Yang J, Ariel P, Tessier-Lavigne M. 2014. iDISCO: A simple, rapid method to immunolabel large tissue samples for volume imaging. *Cell* 159:896–910

Schnell SA, Staines WA, Wessendorf MW. 1999. Reduction of lipofuscin-like autofluorescence in fluorescently labeled tissue. *J. Histochem. Cytochem.* 47:719–30

Schwarz MK, Scherbarth A, Sprengel R, Engelhardt J, Theer P, Giese G. 2015. Fluorescent-protein stabilization and high-resolution imaging of cleared, intact mouse brains. *PLOS ONE* 10:e0124650

Sealy R, Felix C, Hyde J, Swartz H. 1980. Structure and reactivity of melanins: influence of free radicals and metal ions. *Free Radic. Biol.* 4:209–59

Sharpe J. 2004. Optical projection tomography. *Annu. Rev. Biomed. Eng.* 6:209–28

Shimomura O. 1979. Structure of the chromophore of *Aequorea* green fluorescent protein. *FEBS Lett.* 104:220–22

Shimomura O, Johnson FH, Saiga Y. 1962. Extraction, purification and properties of aequorin, a bioluminescent protein from luminous hydromedusan, *Aequorea*. *J. Cell. Comp. Physiol.* 59:223–39

Shokeen M, Anderson CJ. 2009. Molecular imaging of cancer with copper-64 radiopharmaceuticals and positron emission tomography (PET). *Acc. Chem. Res.* 42:832–41

Shu X, Shaner NC, Yarbrough CA, Tsien RY, Remington SJ. 2006. Novel chromophores and buried charges control color in mFruits. *Biochemistry* 45:9639–47

Sompuram SR, Vani K, Messana E, Bogen SA. 2004. A molecular mechanism of formalin fixation and antigen retrieval. *Am. J. Clin. Pathol.* 121:190–99

Spalteholz W. 1914. *Über das Durchsichtigmachen von menschlichen und tierischen Präparaten*. Leipzig, Ger.: S. Hirzel

Staudt T, Lang MC, Medda R, Engelhardt J, Hell SW. 2007. 2,2′-Thiodiethanol: a new water soluble mounting medium for high resolution optical microscopy. *Microsc. Res. Tech.* 70:1–9

Steinke H, Wolff W. 2001. A modified Spalteholz technique with preservation of the histology. *Ann. Anat.* 183:91–95

Stepanenko OV, Stepanenko OV, Kuznetsova IM, Shcherbakova DM, Verkhusha VV, Turoverov KK. 2012. Distinct effects of guanidine thiocyanate on the structure of superfolder GFP. *PLOS ONE* 7:e48809

Susaki EA, Tainaka K, Perrin D, Kishino F, Tawara T, et al. 2014. Whole-brain imaging with single-cell resolution using chemical cocktails and computational analysis. *Cell* 157:726–39

Susaki EA, Tainaka K, Perrin D, Yukinaga H, Kuno A, Ueda HR. 2015. Advanced CUBIC protocols for whole-brain and whole-body clearing and imaging. *Nat. Protoc.* 10:1709–27

Susaki EA, Ueda HR. 2016. Whole-body and whole-organ clearing and imaging techniques with single-cell resolution: toward organism-level systems biology in mammals. *Cell Chem. Biol.* 23:137–57

Sylwestrak EL, Rajasethupathy P, Wright MA, Jaffe A, Deisseroth K. 2016. Multiplexed intact-tissue transcriptional analysis at cellular resolution. *Cell* 164:792–804

Tainaka K, Kubota SI, Suyama TQ, Susaki EA, Perrin D, et al. 2014. Whole-body imaging with single-cell resolution by tissue decolorization. *Cell* 159:911–24

Teale FW. 1959. Cleavage of the haem-protein link by acid methylethylketone. *Biochim. Biophys. Acta* 35:543

Tomer R, Ye L, Hsueh B, Deisseroth K. 2014. Advanced CLARITY for rapid and high-resolution imaging of intact tissues. *Nat. Protoc.* 9:1682–97

Treweek JB, Chan KY, Flytzanis NC, Yang B, Deverman BE, et al. 2015. Whole-body tissue stabilization and selective extractions via tissue-hydrogel hybrids for high-resolution intact circuit mapping and phenotyping. *Nat. Protoc.* 10:1860–96

Tsien RY. 1998. The green fluorescent protein. *Annu. Rev. Biochem.* 67:509–44

Tuchin VV. 2015. Tissue optics and photonics: light-tissue interaction. *J. Biomed. Photonics Eng.* 1:98–134

Tuchin VV, Maksimova IL, Zimnyakov DA, Kon IL, Mavlyutov AH, Mishin AA. 1997. Light propagation in tissues with controlled optical properties. *J. Biomed. Opt.* 2:401–17

Usha R, Ramasami T. 2002. Effect of hydrogen-bond-breaking reagent (urea) on the dimensional stability of rat tail tendon (RTT) collagen fiber. *J. Appl. Polym. Sci.* 84:975–82

Ward WW, Prentice HJ, Roth AF, Cody CW, Reeves SC. 1982. Spectral perturbations of the *Aequorea* green-fluorescent protein. *Photochem. Photobiol.* 35:803–8

Warner CA, Biedrzycki ML, Jacobs SS, Wisser RJ, Caplan JL, Sherrier DJ. 2014. An optical clearing technique for plant tissues allowing deep imaging and compatible with fluorescence microscopy. *Plant Physiol.* 166:1684–87

Weissleder R. 2001. A clearer vision for in vivo imaging. *Nat. Biotechnol.* 19:316–17

Xiong H, Zhou Z, Zhu M, Lv X, Li A, et al. 2014. Chemical reactivation of quenched fluorescent protein molecules enables resin-embedded fluorescence microimaging. *Nat. Commun.* 5:3992

Yang B, Treweek JB, Kulkarni RP, Deverman BE, Chen CK, et al. 2014. Single-cell phenotyping within transparent intact tissue through whole-body clearing. *Cell* 158:945–58

Yarbrough D, Wachter RM, Kallio K, Matz MV, Remington SJ. 2001. Refined crystal structure of DsRed, a red fluorescent protein from coral, at 2.0-Å resolution. *PNAS* 98:462–67

Zimmerman SB, Minton AP. 1993. Macromolecular crowding: biochemical, biophysical, and physiological consequences. *Annu. Rev. Biophys. Biomol. Struct.* 22:27–65